Transcriptomic and epigenomic consequences of heterozygous loss of function mutations in *AKAP11*, the first large-effect shared risk gene for bipolar disorder and schizophrenia

Nargess Farhangdoost[1,2], Calwing Liao[3,4,5], Yumin Liu[2,6], Martin Alda[7], Patrick A. Dion[1,2,6], Guy A. Rouleau[1,2,6#], Anouar Khayachi[2,6#], and Boris Chaumette[8,9#]

1 Department of Human Genetics, McGill University, Montreal, Quebec, Canada

2 Montreal Neurological Institute and Hospital, Montreal, Quebec, Canada

3 Analytic and Translational Genetics Unit, Massachusetts General Hospital, Boston, MA, USA

4 Stanley Center for Psychiatric Research, Broad Institute of MIT and Harvard, Cambridge, MA, USA

5 Department of Medicine, Harvard Medical School, Boston, MA, USA

6 Department of Neurology & Neurosurgery, McGill University, Montreal, Quebec, Canada

7 Department of Psychiatry, Dalhousie University, Halifax, Nova Scotia, Canada

8 Université Paris Cité, Institute of Psychiatry and Neuroscience of Paris (INSERM U1266), GHU Paris Psychiatrie et Neurosciences, Paris, France

9 Department of Psychiatry, McGill University, Montreal, Quebec, Canada

#Corresponding authors

Abstract

The gene A-kinase anchoring protein 11 (*AKAP11*) recently emerged as a shared risk factor between bipolar disorder and schizophrenia, driven by large-effect loss-of-function (LoF) variants. Recent research has uncovered the neurophysiological characteristics and synapse proteomics profile of *Akap11*-mutant mouse models. Considering the role of AKAP11 in binding cAMP-dependent protein kinase A (PKA) and mediating phosphorylation of numerous substrates, such as transcription factors and epigenetic regulators, and given that chromatin alterations have been implicated in the brains of patients with bipolar disorder and schizophrenia, it is crucial to uncover the transcriptomic and chromatin dysregulations following the heterozygous knockout of *AKAP11*, particularly in human neurons. In this study, we use genome-wide approaches to investigate such aberrations in human induced pluripotent stem cell (iPSC)-derived neurons. We show the impact of heterozygous *AKAP11* LoF mutations on the gene expression landscape and profile the methylomic and acetylomic modifications. Altogether we highlight the involvement of aberrant activity of intergenic and intronic enhancers, which are enriched in PBX homeobox 2 (PBX2) and Nuclear Factor-1 (NF1) known binding motifs, respectively, in transcription dysregulations of genes functioning as DNA-binding transcription factors, actin and cytoskeleton regulators, and cytokine receptors, as well as genes involved in G-protein-coupled receptors (GPCRs) binding and signaling. A better understanding of the dysregulations resulting from haploinsufficiency in *AKAP11* improves our knowledge of the biological roots and pathophysiology of BD and SCZ, paving the way for better therapeutic approaches.

Introduction

Bipolar disorder (BD) is a complex, severe psychiatric disorder with a lifetime prevalence of 2-3% in the general population[1,2,4,5]. BD is characterized by recurrent episodes of mania and depression and is often accompanied by psychotic symptoms, resembling those observed in schizophrenia (SCZ)[3,4], and considerable clinical comorbidities [1-5]. Despite extensive research, the etiology of BD remains largely unknown. Recent studies have underscored the significance of protein-truncating variations (PTVs) and copy number variations (CNVs) in BD[6,7]. Most recently, the Bipolar Exome (BipEx) consortium, involving whole-exome sequencing of 13,933 BD cases and 14,422 controls, identified *AKAP11* as a significant rare-variant risk gene for BD[3]. *AKAP11* was found to be enriched in rare protein-truncating variations, significantly elevating the risk for BD and establishing it as the strongest known risk gene for BD to date[3]. Notably, this genetic risk factor is shared between BD and SCZ (combined odds ratio [OR] = 7.06, p = 2.83 × 10E−9)[3].

Generally, A-kinase anchoring proteins (AKAPs) bind to PKA regulatory subunits as well as cytoskeleton proteins or organelles[8,9], which allows for their pivotal role in distributing and localizing PKA to its targets within the cells[8,9]. They are now understood to have multiple binding sites for various signaling molecules, such as protein kinase C, protein phosphatases, GPCRs, adenylyl cyclases, and phosphodiesterases[10-13]. In neurons, AKAPs localize these signaling enzymes to their substrates allowing precise temporal and spatial interactions among postsynaptic signaling molecules, impacting synaptic plasticity and neuronal function[10-13]. AKAP11 is a ubiquitously expressed membrane-associated and vesicular anchoring protein that is under LoF constraint (LOEUF = 0.32, pLI =1 on gnomAD v4.0) and is highly expressed in the brain tissue[14]. It binds to type II regulatory subunits of PKA and regulates the interaction between PKA and its numerous substrates[15,16]. AKAP11's interaction with PKA leads to the localization of this complex to its substrates, e.g., Glycogen Synthase Kinase 3 Beta (GSK3B[17], a molecular target of lithium which is widely used to treat BD[18-21]), IQ motif-containing GTPase-activating protein 2 (IQGAP2)[22], and protein phosphatase-1 (PP1)[17,23], regulating their functions. AKAP11-mediated phosphorylation of substrates through PKA can affect a plethora of events, including signaling pathways, regulation of transcription factors, e.g., cAMP-response element binding (CREB) [24], and modulation of epigenetic regulators, e.g., histone deacetylases (HDACs)[25,26]. In addition, AKAP11 has been suggested to interact with other proteins including transcription factors and epigenetics regulators, e.g., SET and MYND domain containing 2 (SMYD2/KMT3C)[27-29] and Iroquois Homeobox 3 (IRX3)[30]. Owing to such potential direct or indirect effects of AKAP11 on the regulation of chromatin accessibility and gene expression, it is important to understand the transcriptomic and epigenomic consequences of heterozygous LoF of *AKAP11* and identify the key processes that overlap with our current knowledge of the etiology of BD and SCZ.

Recently, heterozygous *Akap11* mouse mutants were generated and screened for identification of a neurophysiological biomarker, i.e. electroencephalography (EEG) phenotypes similar to those observed in human SCZ patients were detected[31-33]. Another study carried out a deep proteomics analysis of synapses in *Akap11*-mutant mice and detected some overlap between the dysregulated pathways in SCZ and BD patients and the mutant model[34]. However, our study is the first to investigate the effect of heterozygous LoF mutations in *AKAP11* at the transcriptomic

and epigenetic (DNA methylation and histone modification) levels in a human cellular model. A better understanding of the dysregulations resulting from AKAP11 haploinsufficiency may improve our knowledge of the biological roots and pathophysiology of BD and SCZ, eventually contributing to improved diagnosis and therapeutic approaches.

To investigate the transcriptomic and epigenetic consequences of heterozygous LoF of AKAP11, we employed a human iPSC, reprogrammed from lymphoblastoid cells derived from an unaffected individual[35,36]. Subsequently, three heterozygous *AKAP11*-Knockout (*AKAP11*-KO) isogenic clones were created from the iPSC, each harboring a different heterozygous frameshift mutation using CRISPR-Cas9 genome editing. We then differentiated these into 25-day-old neurons and compared their respective transcriptome to the one of WT counterpart neurons. Gene set enrichment analysis (GSEA) highlighted downregulation of genes related to ribosome function and DNA-binding transcription factor activity, and upregulation in molecular functions including signaling receptor interactions, cytokine activity, and cytoskeletal dynamics. Using whole-genome bisulfite sequencing (WGBS) we identified the differentially methylated regions (DMRs) and found an overlap between the genes associated with DMRs and genes with differential expression. These overlapping genes were enriched in GO terms related to DNA-binding transcription factor activity. Examination of enhancer activity in heterozygous *AKAP11*-KO iPSC-derived neurons, using chromatin immunoprecipitation followed by sequencing (ChIP-seq) of histone H3 Lysine 27 acetylation (H3K27ac) mark, revealed that reduced intergenic enhancer activity play a partial role in downregulation of neighboring genes involved in transcription factor binding and activity. Conversely, elevated intronic enhancer activity partly accounts for the upregulation of genes involved in signaling receptor binding, cytokine receptor binding, and cytoskeleton-related functions. Furthermore, we found significant enrichment of GPCR binding and signaling terms among differentially expressed genes (DEGs) in *AKAP11*-KO, as well as among genes associated with DMRs. While DMRs did not seem to particularly influence the transcription of genes involved in such pathways, a portion of such gene expression dysregulations was linked to enhancer activity alterations. Lastly, we investigated the correlation between the DMRs and enhancer activity alterations, marked by H3K27ac, and subsequently pinpointed the most profoundly impacted intergenic and intronic regulatory regions linked to concordant gene expression dysregulations, resulting from heterozygous LoF mutations in *AKAP11*.

Materials / Subjects and Methods

Ethics statement

The cell line and protocols in the present study were used in accordance with guidelines approved by the institutional human ethics committee guidelines and the Nova Scotia Health Authority Research Ethics Board (REB # 1020604).

RNP-CRISPR-Cas9 knockout of *AKAP11* in induced pluripotent stem cells

The iPSCs used in this study were reprogrammed from the lymphoblasts (blood sample) of a consenting individual [35,36] (Table 1). We utilized a control iPSC line (SBP009, male, age 53, Caucasian; Table 1) to knock out *AKAP11*, using the RNP-CRISPR-Cas9 genome editing technique. To generate three isogenic knockout clones from the WT iPSC (SBP009), Ribonucleoprotein (RNP)-mediated CRISPR-Cas9 genome editing was performed using the Alt-R CRISPR-Cas9 system (IDT). Two synthetic crRNA guides were designed (TACTGGTATAAGGTACACCT PAM:TGG and CTGATGCAAGAATGTGTCCA PAM:AGG) to form a duplex with Alt-R® CRISPR-Cas9 tracrRNA, ATTO 550 (IDT, Cat. # 1075928) and coupled to the Alt-R© S.p. Cas9 Nuclease V3 (IDT). The Lipofectamine™ Stem Transfection (Invitrogen, Cat. #STEM00001) and PLUS™ Reagent (Invitrogen, Cat. #11514015) ratios were optimized with a lower volume than the manufacturer's protocol. The transfected cells were incubated for 48 hours. Single ATTO550+ cells were then sorted into 96-well plates. Clones were expanded and individually verified with MiSeq sequencing of the target loci using the following primers: fwLeft: CCAAGGAGCTTTTCAGGATGC and fwRight: TGGTCTCAAGTTGGTGCTTCT. All the clones were also kept frozen at the NPC stage in FBS (Gibco, Cat. #12484028) +10% DMSO (Sigma, Cat. #D2650) at the lowest passage possible for future use. The control group consists of three replicates of SBP009 iPSCs at different passage numbers that were separately induced into NPCs, through separate EB formation and rosette selection processes. These NPCs were then differentiated into 25-day-old neurons using the same protocol, as described below.

Sample	Source	Reference	Identifier	Clinical information of the donor
Induced Pluripotent Stem Cell (iPSC)	Human lymphoblasts	Sample generously given to us by Dr. Martin Alda; Reprogrammed into iPSC by Sanford Burnham[35,36].	SBP009	Control, Unaffected individual, Male, 51, Caucasian.

Table1. Details of the iPSC sample used in the study.

iPSC and NPC differentiation and maintenance and neuronal cell culture

iPSCs were maintained on a Matrigel (Corning, Cat. #08-774-552) coated plate with mTeSR™1 medium (STEMCELL Technologies, Cat. #85870) along with Y-27632 (ROCK inhibitor, STEMCELL Technologies, Cat. # 72307) after each passage. During the course of induction of iPSC to NPCs (20 days), STEMdiff™ SMADi Neural Induction Kit (STEMCELL

Technologies, Cat. #08581) was used. The method for induction of iPSC to NPCs was based on the STEMCELL™ neural induction EB-based method and was performed following the manufacturer's protocol. On Day 0, a single-cell suspension of iPSC was generated using Gentle Cell Dissociation Reagent (STEMCELL Technologies, Cat. # 100-0485), and 10,000 cells per microwell were seeded in an ultralow attachment 96-well plate to generate Embryoid bodies (EBs), cultured in STEMdiff™ Neural Induction Medium + SMADi (STEMdiff™ SMADi Neural Induction Kit, Cat. # 08582) + 10 µM Y-27632. From Day 1 to Day 4, a daily partial (3/4) medium change was performed using STEMdiff™ Neural Induction Medium + SMADi. On Day 5, EBs were harvested using a wild-board 1ml serological pipettes and 40µm strainer and transferred to a single well of a 6-well plate coated with Poly-L-ornithine hydrobromide (PLO) and laminin. A daily full medium change was performed from Day 6 to Day 11. After the neural induction efficiency was determined higher than 75%, neural rosettes were manually selected using STEMdiff™ Neural Rosette Selection Reagent (STEMCELL Technologies, Cat. # 05832) on Day 12 and replated onto a single well of PLO/Laminin coated 6-well plate. With continuous daily full medium change, selected rosette-containing clusters attached, and NPC outgrowths formed a monolayer between the clusters. The NPCs were ready for passage 1 when cultures were approximately 80 - 90% confluent (typically on Day 19). NPCs were maintained and expanded (7-10 days) using DMEM/F12 with Glutamax (ThermoFisher, Cat. #10565042), N2 1x (ThermoFisher, Cat. # 17502001), B27 1x (ThermoFisher, Cat. #17504001), FGF2 20 ng/ml (PEPROTECH, Cat. #100-18B), and EGF 20 ng/ml (Gibco, Cat. # AF-100-15-1MG). For the final differentiation of NPCs into neurons, NPCs were detached using Accutase (STEMCELL Technologies, Cat. #7922) and then differentiated onto PLO/laminin-coated plates with final differentiation media of BrainPhys™ Neuronal Medium (STEMCELL Technologies, Cat. #05790) supplemented with Glutamax 1x (ThermoFisher, Cat. #35050061), N2 1x (ThermoFisher, Cat. #17502001), B27 1x (ThermoFisher, Cat. #17504001), 200nM ascorbic acid 200nM (STEMCELL Technologies, Cat. #72132), cyclic AMP 500 µg/ml (Sigma-Aldrich, Cat #A9501-1G), brain-derived neurotrophic factor 20 ng/ml (BDNF, GIBCO, Cat. #PHC7074), Wnt3a 10 ng/ml (R&D Systems, Cat. #5036-WN-500), and laminin 1 µg/ml (Gibco, Cat. #23017015) for 14 days (medium change of 3 times per week). Subsequently, the cells were maintained in STEMdiff™ Forebrain Neuron Maturation Kit for 11 days (STEMCELL Technologies, Cat. #08605) --final differentiation media was replaced by STEMdiff™ Forebrain Neuron Maturation Kit in the same dishware.

Reverse-transcription quantitative PCR (RT-qPCR)

To confirm the lower *AKAP11* expression in KOs compared to the parental, reverse-transcription quantitative PCR (RT-qPCR) was performed on neurons using a pre-design assay from ThermoScientific (Cat. #4351372, Assay ID: Hs01568657_g1, Ref gene: *POLR2A*) targeting *AKAP11* exon 7, where the CRISPR-Cas9 guide sites were located. RNA extraction was performed using RNeasy kit Qiagen (Cat. #74004) according to the manufacturer's instructions.

Neuronal immunocytochemistry

iPSC-derived neurons were fixed in phosphate-buffered saline (PBS) containing 5% sucrose and 3.7% formaldehyde for 1 h at room temperature (RT). They were then permeabilized with the same buffer but with 0.2% Triton 100x for 2 minutes at RT. The cells were rinsed twice with PBS 1x at RT and incubated with NH4CI (50mM) in PBS for 10 minutes at RT. They were then rinsed with PBS 1x twice. It was ensured that the coverslip did not dry out. The cells were incubated in PBS1x / goat serum (GS) 10% for 20 minutes at RT. Primary antibody (BIII-Tubulin from Sigma-Aldrich (mouse, Cat. #T8660)) along with DAPI (Abcam; Cat. #ab228549) were added to the cells in PBS 1x / 5% GS / 0.05% Triton 100x and were incubated overnight at 4°C. The cells were then washed three times (5 minutes each) with PBS 1x at RT. The appropriate secondary antibody (1/1000) conjugated to Alexa488 (Invitrogen, Cat. #A21202) was added to the cells in PBS 1x / 5% GS / 0.05% Triton 100x and incubated for 45 minutes at RT. The cells were then washed three times with PBS at RT and once with ddH2O. Finally, the coverslip was mounted with Prolong (ThermoFisher, Cat. #P36930) until confocal examination. The images (1024 × 1024) were acquired with a ×20 lens (numerical aperture NA 1.4) on an SP8 confocal microscope (Leica Microsystems) and were visualized using image j (FIJI).

RNA-seq library Preparation and Sequencing

RNA was extracted from bulk neuronal culture 25 days post-differentiation using RNeasy Mini Kit (Cat. #74104). Library preparation from total RNA was performed using NEB rRNA-depleted (HMR) stranded library preparation kit according to the manufacturer's instructions and sequencing was carried out using Illumina NovaSeq 6000 (100 bp paired-end).

WGBS library preparation and sequencing

DNA was extracted from bulk neuronal culture 25 days post-differentiation using DNeasy Blood & Tissue Kit (Cat. #69504). Whole genome sequencing libraries were generated from 1000 ng of genomic DNA spiked with 0.1% (w/w) unmethylated λ DNA (Roche Diagnostics) and fragmented to 300–400 bp peak sizes using the Covaris focused-ultrasonicator E210. Fragment size was controlled on a Bioanalyzer High Sensitivity DNA Chip (Agilent) and NxSeq AmpFREE Low DNA Library Kit (Lucigen) was applied. End repair of the generated dsDNA with 3' or 5' overhangs, adenylation of 3' ends, adaptor ligation, and clean-up steps were carried out as per Lucigen's recommendations. The cleaned-up ligation product was then analyzed using LabChip GX/GX II (Caliper). Samples were then bisulfite converted using the EZ-DNA Methylation Gold Kit (Zymo Research) according to the manufacturer's protocol. DNA was amplified by 9 cycles of PCR using the Kapa HiFi Uracil+ Kit (Roche) DNA polymerase (KAPA Biosystems) according to the manufacturer's protocol. The amplified libraries were purified using Ampure XP Beads (Beckman Coulter), validated on LabChip GX/GX II (Caliper), and quantified by qPCR amplification with Illumina adapters. The values are read using Lightcycler LC480 (Roche). Sequencing of the WGBS libraries was performed on the Illumina NovaSeq6000 S4 v1.5 using 150-bp paired-end sequencing.

Cross-linking, ChIP-seq library preparation, and sequencing

About 10 million neuronal cells per sample (3 heterozygous *AKAP11*-KO clones and 3 WT replicates) were grown and directly crosslinked on the plate with 1% formaldehyde (Sigma) for 10 minutes at room temperature and the reaction was stopped using 125nM Glycine for 5 minutes. Fixed cell preparations were washed with ice-cold PBS, scraped off the plate, pelleted, washed twice again in ice-cold PBS, and the flash-frozen pellets were stored at −80°C.

Thawed pellets were resuspended in 500ul cell lysis buffer (5 mM PIPES-pH 8.5, 85 mM KCl, 1% (v/v) IGEPAL CA-630, 50 mM NaF, 1 mM PMSF, 1 mM Phenylarsine Oxide, 5 mM Sodium Orthovanadate, EDTA-free Protease Inhibitor tablet) and incubated 30 minutes on ice. Samples were centrifugated and pellets resuspended in 500ul of nuclei lysis buffer (50 mM Tris-HCl pH 8.0, 10 mM EDTA, 1% (w/v) SDS, 50 mM NaF, 1 mM PMSF, 1 mM Phenylarsine Oxide, 5 mM Sodium Orthovanadate and EDTA-free protease inhibitor tablet) and incubated 30 minutes on ice. Sonication of lysed nuclei was performed on a BioRuptor UCD-300 at max intensity for 45 cycles, 10 s on 20 s off, centrifuged every 15 cycles, and chilled by a 4°C water cooler. Samples were checked for sonication efficiency using the criteria of 150–500bp by gel electrophoresis of a reversed cross-linked and purified aliquot. After the sonication, the chromatin was diluted to reduce the SDS level to 0.1% and concentrated using Nanosep 10k OMEGA (Pall). ChIP reaction for histone modifications was performed on a Diagenode SX-8G IP-Star Compact using Diagenode automated Ideal ChIP-seq Kit for Histones. Dynabeads Protein A (Invitrogen) were washed, then incubated with specific antibodies (rabbit polyclonal anti-H3K27ac Diagenode Cat. #C15410196, RRID: AB_2637079), 1 million cells of sonicated cell lysate, and protease inhibitors for 10 hr, followed by 20 min wash cycle using the provided wash buffers (Diagenode Immunoprecipitation Buffers, iDeal ChIP-seq kit for Histone).

Reverse cross-linking took place on a heat block at 65°C for 4 hr. ChIP samples were then treated with 2ul RNase Cocktail at 65°C for 30 min followed by 2ul Proteinase K at 65°C for 30 min. Samples were then purified with QIAGEN MinElute PCR purification kit (QIAGEN) as per manufacturers' protocol. In parallel, input samples (chromatin from about 50,000 cells) were reverse crosslinked, and DNA was isolated following the same protocol. Library preparation was carried out using Kapa Hyper Prep library preparation reagents (Kapa Hyper Prep kit, Roche 07962363001) following the manufacturer's protocol. ChIP libraries were sequenced using Illumina NovaSeq 6000 at 100bp paired-end reads.

RNA-seq data processing and analysis

Adaptor sequences and low-quality score bases (Phred score < 30) were first trimmed using Trimmomatic[37]. The resulting reads were aligned to the GRCh38 human reference genome assembly, using STAR[38]. Read counts were obtained using HTSeq[39] with parameters-m intersection-nonempty-stranded=reverse. For all downstream analyses, we excluded lowly expressed genes with an average read count lower than 20 across all samples, resulting in a total of 23,590 genes. Raw counts were normalized using edgeR's TMM algorithm[40] and were then transformed to log2-counts per million (logCPM) using the voom function implemented in the limma R package[41].

To assess differences in gene expression levels between the different conditions (3 KOs versus 3 WT replicates), we fitted a linear model using limma's lmfit function with parameter method="robust". Nominal p-values were corrected for multiple testing using the Benjamini-Hochberg method.

The Z-score heatmap was constructed using the R package ComplexHeatmap[42]; KO vs WT analysis: P-adj < 0.05 & | log2FC| > 1.

Gene set enrichment analysis (GSEA) based on a pre-ranked gene list by t-statistic was performed using the R package fgsea (http://bioconductor.org/packages/fgsea), P-adj < 0.05. Over-representation analysis (ORA) was performed using ShinyGO 0.77[43] (http://bioinformatics.sdstate.edu/go) and FDR<0.05. The background genes used for ORA were all the 23,590 genes that were considered expressed. FDR is calculated based on the nominal P-value from the hypergeometric test. Fold Enrichment is the percentage of genes in the input gene list belonging to a pathway divided by the corresponding percentage in the background.

For visualization, gene expression data was corrected for batch effects using ComBat[44]. WGBS data processing and analysis

Adaptor sequences and low-quality score bases were first trimmed using Trimmomatic[37]. The resulting reads were mapped to the human reference genome (GRCh38) and lambda phage genome using Bismark[45], which uses a bisulfite-converted reference genome for read mapping. Only reads that had a unique alignment were retained and PCR duplicates were marked using Picard tools (https://broadinstitute.github.io/picard/). Methylation levels for each CpG site were estimated by counting the number of sequenced C ('methylated' reads) divided by the total number of reported C and T ('unmethylated' reads) at the same position of the reference genome using Bismark's methylation extractor tool. We performed a strand-independent analysis of CpG methylation where counts from the two Cs in a CpG and its reverse complement (position on the plus strand and position i+1 on the minus strand) were combined and assigned to the position of the C in the plus strand. To assess MethylC-seq bisulfite conversion rate, the frequency of unconverted cytosines (C basecalls) at lambda phage CpG reference positions was calculated from reads uniquely mapped to the lambda phage reference genome. CpG sites with at least 5X coverage were included for all downstream analyses. Differential methylation analyses were performed using the R (R 4.1.2, https://www.r-project.org/) package DSS (DMLfit.multiFactor function with parameter smoothing = TRUE)[46]. DMRs were called using the function callDMR at default parameters with a minimum length of 50 base pairs and 3 CpG sites (delta=0, p.threshold=1e-5, minlen=50, minCG=3, dis.merge=100, pct.sig=0.5). Annotation determined using Homer (hg38)[47]. Methylation values and P-values are averaged within each DMR.

Over-representation analysis of genes assigned to DMRs was performed using ShinyGO 0.77[43] (http://bioinformatics.sdstate.edu/go) with FDR>0.05. The background genes used for ORA were the same background gene list (23,590 genes) obtained from our RNA-seq analysis. FDR is calculated based on the nominal P-

value from the hypergeometric test. Fold Enrichment is the percentage of genes in the input gene list belonging to a pathway divided by the corresponding percentage in the background.

ChIP-seq data processing and analysis

ChIP-seq reads were first trimmed for adapter sequences and low-quality score bases using Trimmomatic[37]. The resulting reads were mapped to the human reference genome (GRCh38) using BWA-MEM[48] in paired-end mode at default parameters. Only reads that had a unique alignment (mapping quality > 20) were retained and PCR duplicates were marked using Picard tools (http://broadinstitute.github.io/picard/). Peaks were called using MACS2[49].

To detect changes in histone modifications, a consensus peak set for H3K27ac was first generated by merging ChIP-seq peaks across samples using bedtools merge (https://bedtools.readthedocs.io/). A peak must be present in at least one sample in either condition. Read counts were obtained within these genomic regions using HOMER. Differential peak analysis was performed using the R package limma[41]. Nominal p-values were corrected for multiple testing using the Benjamini-Hochberg method.

Peaks were associated with the nearest TSS of genes using the annotatePeaks command from HOMER software suite [47]. Enrichment analysis (ORA) of genes assigned to differential peaks was performed using ShinyGO 0.77[43] (http://bioinformatics.sdstate.edu/go). The background genes used for ORA were the same background gene list (23,590 genes) obtained from our RNA-seq analysis. FDR is calculated based on the nominal P-value from the hypergeometric test. Fold Enrichment is the percentage of genes in the input gene list belonging to a pathway divided by the corresponding percentage in the background. Motif enrichment within differential peaks was performed using the HOMER findMotifsGenome command. We only included genes/peaks that are associated within 100 kb (distance of 100 kb from the TSS to the peak center) and have concordant changes in expression/histone mark.

Bigwig coverage files were created with the HOMER makeUCSCfile command and bedGraphToBigWig utility from UCSC. Data were normalized so that each value represents the read count per base pair per 10 million reads. Heatmaps and average profiles were generated using modules “computeMatrix” (--referencePoint center) followed by “plotHeatmap” and “plotProfile” from deepTools[50], using bigwig files as input.

Results

Heterozygous *AKAP11* knockout in human iPSCs and generation of iPSC-derived neurons

Using a human iPSC, from the lymphoblasts of an unaffected individual[35,36], we generated 3 heterozygous *AKAP11*-knockout (*AKAP11*-KO) isogenic neuronal clones, each carrying a different heterozygous frameshift mutation (Figure 1A). We then validated the heterozygous *AKAP11*-KO isogenic clones (at the iPSC level) using Miseq amplicon sequencing. Among the individual clones obtained, clone #16 has an 11 bp-deletion, clone #20 has a 10 bp-deletion, and clone #21 has a 4 bp-insertion (Supplementary Figure 1A). Additionally, we performed a KaryoStat+ assay for digitally visualizing any probable chromosomal aberrations in the genetically edited iPSC clones, and we confirmed that there are no chromosomal aberrations in the isogenic heterozygous *AKAP11*-KO iPSC clones compared to their WT counterpart (Supplemental Figure 1B). Subsequently, the *3* heterozygous *AKAP11*-KO iPSC clones, along with 3 replicates of their parental iPSC counterparts (WT; SBP009) were induced into neural progenitor cells (NPCs) and were then differentiated into forebrain neurons of age 25 days (Figure 1A; both groups of neurons were collected on day 25). After collecting the neurons, we carried out RT-qPCR to ensure the gene expression level changes of the heterozygous *AKAP11*-KO clones compared to the WT counterpart in the neuronal context and observed significantly lower expression levels of the heterozygous *AKAP11*-KO clones compared to the WT parental. Clones 16 and 21 had a 0.4-fold and clone 20 had a 0.6-fold decrease in *AKAP11* expression of exon 7 (Figure 1B). We then performed Neuronal Immunocytochemistry and stained the heterozygous *AKAP11*-KO and WT neurons with BIII-Tubulin, a neuronal marker, and DAPI and confirmed the presence of a viable neuronal culture broadly expressing BIII-Tubulin (Figure 1C). This ensures that the heterozygous knockout of *AKAP11* does not disturb the neuronal culture differentiation and viability. Further cell type deconvolution using bulk RNA sequencing (RNA-seq) data and dtangle method[51] confirmed the presence of neurons as the most abundant cell type in our cultures for both heterozygous *AKAP11*-KO and WT samples (Supplementary Figure 1C).

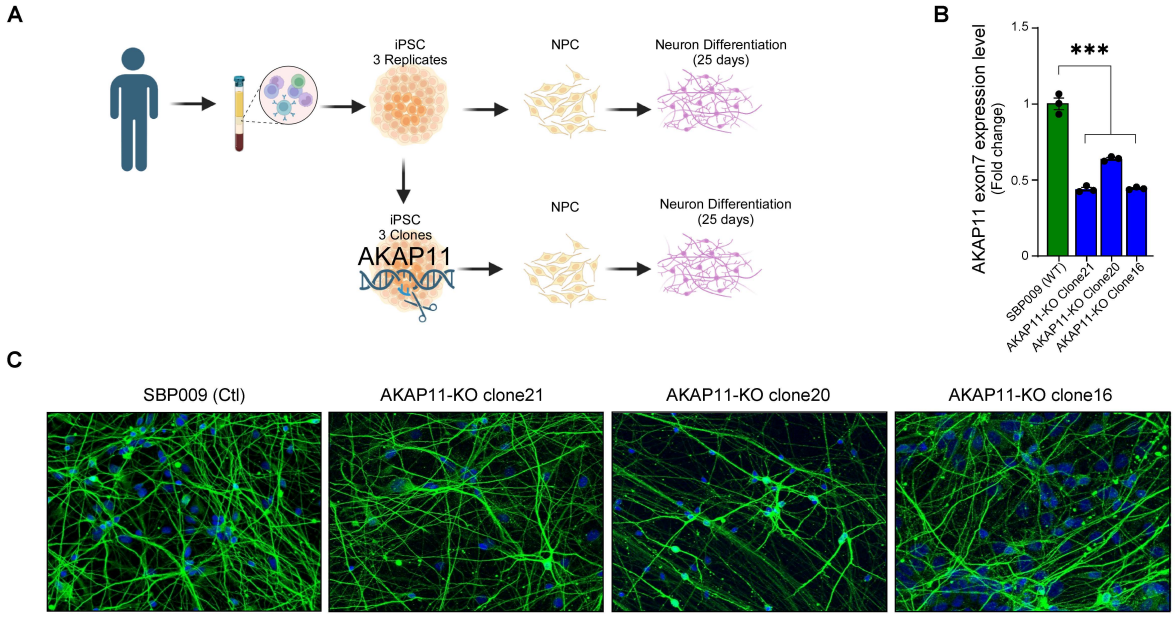

Figure 1. iPSC differentiation into neurons, validation of *AKAP11*-KO, and culture viability. A) Schematic view of the origin and differentiation steps of iPSC-derive neurons as well as heterozygous knockout of *AKAP11* at iPSC level. **B**) R T-qPCR gene expression level changes of exon 7 of the *AKAP11*-KO clones and WT (SBP009). Each clone was processed as triplicates along with an endogenous control (POLR2A). Data shown in this figure are the mean ± s.e.m. and statistical significance determined by one-way ANOVA with Bonferroni post-test. ****p<0.0001. **C**) Neuronal Immunocytochemistry of *AKAP11*-KO iPSC-derived neuronal clones at day 25 post-differentiation. BIII-Tubulin: Green, DAPI: Blue.

Transcriptomic changes and biological pathways affected by heterozygous LoF of *AKAP11* in iPSC-derived neurons

Using the gene expression data from RNA-seq, we identified DEGs resulting from heterozygous *AKAP11*-KO vs. WT comparison with the p-adjusted value of (p-adj) < 0.05 and |log2FC| > 1 (Figure 2A, Supplementary Table 1). A total of 849 genes showed significant differential expression out of which 421 genes were downregulated, and 428 were upregulated (Figure 2B). Hierarchical clustering of differentially expressed genes demonstrated a clear separation in gene expression profiles between heterozygous *AKAP11*-KO and WT with the data pattern similarity being high within groups but low between groups (Figure 2C). The top 30 downregulated DEGs, ranked by their p-values, primarily include coding genes and long-noncoding RNA (lncRNA) genes, four of which are located in Prader-Willi syndrome (PWS) region (*PWRN1*, *PWRN4*, *NDN*, *MAGEL2*), and several are related to the homeobox (HOX) gene family (*HOTAIRM1*, *PHOX2A*, *DRGX*, *HOXA2*, *HOXC8*). The top 30 upregulated DEGs include coding and lncRNA genes related to the Wnt signaling pathway (*WIF1*, *WNT2B*), solute carrier (SLC) gene family (*SLC9A3*, *SLC16A4*), and circadian rhythm (*KLF9*, *SIX3*).

We performed over-representation analysis (ORA) using Curated.Reactome[52,53] pathway database to gain a general overview of the main biological pathways that were dysregulated using the obtained DEGs of the heterozygous *AKAP11*-KO vs. WT. We found that the DEGs were highly enriched in GPCR binding and signaling events as well as extracellular matrix (ECM) interactions and focal adhesion-related terms (Figure 2D). The genes that were enriched in the Curated.Reactome term “GPCR ligand binding” included Wnt/Frizzled receptors (*WNT8B*, *WNT2B*, *FZD10*), metabotropic glutamate receptors (GRM3), and Rhodopsin-like receptors (*UTS21*, *CXCL122*, *CCKBR2*, *PTGFR2*, *MCHR12*, *NTS2*, *HTR1B2*, *F2RL22*, *OXGR12*, *BDKRB22*, *GPR372*, *SSTR12*, *CRH2*), among others (Supplementary Figure 2A). GPCRs are the largest family of metabotropic receptors which play a pivotal role in neural communication by regulating synaptic transmission at both pre- and post-synaptic stages[54].

To further extract biological meanings from the gene expression changes resulting from heterozygous *AKAP11*-KO and have a better understanding of their direction of change (up- or downregulated), we performed gene set enrichment analysis (GSEA[55,56]), which ranks the entire gene expression dataset based on t-statistic of each gene's differential expression with respect to the two phenotypes of heterozygous *AKAP11*-KO vs. WT (Figure2F). The entire ranked list was used to evaluate how the genes from the Gene Ontology (GO), molecular function[57,58] are overrepresented at the top or bottom of the ranked list of genes[59]. We showed that, overall, the main downregulated terms were related to ribosome function and protein synthesis as well as transcription regulation, particularly through changes in transcription factor binding activity (Figure 2F, Supplementary Table 2). Gene within the terms related to ribosome function and protein synthesis were mainly ribosomal protein genes and mitochondrial ribosomal protein genes. Furthermore, the transcription factors with differentially decreased expression in heterozygous *AKAP11*-KO were primarily from the family of HOX, Zinc Finger (ZNF), Iroquois homeobox (Irx), Activating transcription factor (ATF), and Paired-box (PAX) (Supplementary Table 2). On the other hand, the top-upregulated GO molecular functions in heterozygous *AKAP11*-KO were involved in diverse molecular functions

including signaling receptor binding, phospholipid binding, postsynaptic Density-95 Discs-large Zona occludens 1 (PDZ)-domain binding, lipid binding, as well as calcium ion- and actin-binding (Figure 2F, Supplementary Table 2). Several of these functions, such as actin-binding, calcium ion binding, SRC Homology 3 (SH3) domain binding, lipid binding, and PDZ domain binding, include genes involved in cell adhesion, cell motility, or cytoskeletal integrity. Overall, the upregulated terms highlighted here are integral to signaling processes, receptor interactions, and cytoskeletal dynamics and are essential for the proper functioning of neurons.

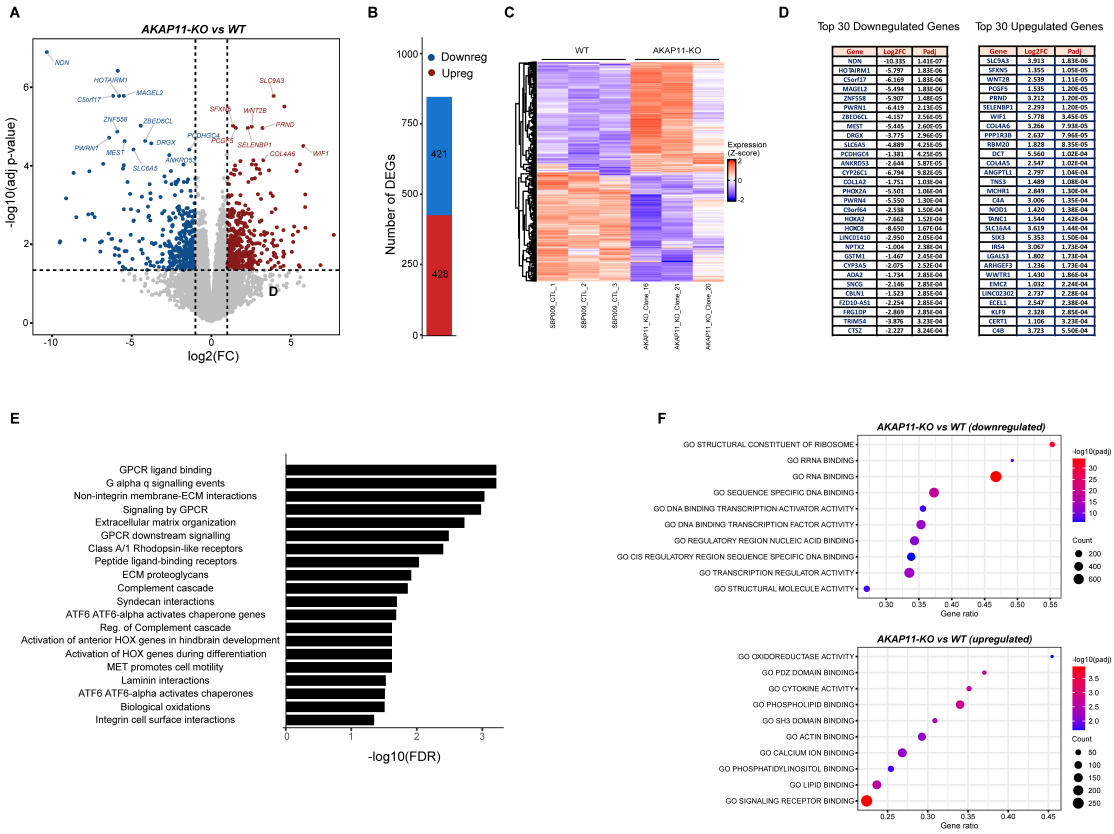

Gene	Log2FC	Padj
NDN	-10.335	1.41E-07
HOTAIRM1	-5.797	1.83E-06
C5orf17	-6.169	1.83E-06
MAGEL2	-5.494	1.83E-06
ZNF558	-5.907	1.48E-05
PWRN1	-6.419	2.13E-05
ZBED6CL	-4.157	2.56E-05
MEST	-5.445	2.60E-05
DRGX	-3.775	2.96E-05
SLC6A5	-4.889	4.25E-05
PCDHGC4	-1.381	4.25E-05
ANKRD53	-2.644	5.87E-05
CYP26C1	-6.794	9.82E-05
COL1A2	-1.751	1.03E-04
PHOX2A	-5.501	1.06E-04
PWRN4	-5.550	1.30E-04
C9orf64	-2.538	1.50E-04
HOXA2	-7.662	1.52E-04
HDHD3	-8.650	1.67E-04
LINC01410	-2.950	2.05E-04
NPTX2	-1.004	2.38E-04
GSTM1	-1.467	2.45E-04
CYP3A5	-2.075	2.52E-04
ADA2	-1.734	2.85E-04
SNCG	-2.146	2.85E-04
CBLN1	-1.523	2.85E-04
FZD10-AS1	-2.254	2.85E-04
FRG1DP	-2.869	2.85E-04
TRIM54	-3.876	3.23E-04
CTSZ	-2.227	3.24E-04

Gene	Log2FC	Padj
SLC9A3	3.913	1.83E-06
SFXN5	1.355	1.05E-05
WNT2B	2.539	1.11E-05
PCGF5	1.535	1.20E-05
PRND	3.212	1.20E-05
SELENBP1	2.293	1.20E-05
WIF1	5.778	3.45E-05
COL4A6	3.266	7.93E-05
PPP1R3B	2.637	7.96E-05
RBM20	1.828	8.35E-05
DCT	5.560	1.02E-04
COL4A5	2.547	1.02E-04
ANGPTL1	2.797	1.04E-04
TNS3	1.489	1.08E-04
MCHR1	2.849	1.30E-04
C4A	3.006	1.35E-04
NOD1	1.420	1.38E-04
TANC1	1.544	1.42E-04
GLCI1GA4	3.619	1.44E-04
SIX3	5.353	1.50E-04
IRS4	3.067	1.73E-04
LGALS3	1.802	1.73E-04
ARHGEF3	1.236	1.73E-04
WWTR1	1.430	1.86E-04
EMC7	1.032	2.24E-04
LINC02302	2.737	2.28E-04
ECEL1	2.547	2.38E-04
KLF9	2.328	2.85E-04
CERT1	1.106	3.23E-04
C4B	3.723	5.50E-04

Figure 2. Identification of DEGs in heterozygous *AKAP11*-KO vs. WT and the pathways/GO terms affected. A) Volcano plot of differentially expressed genes (p-adj < 0.05 and |log2FC| > 1). **B**) Number of up- and down-regulated DEGs. **C**) Heatmap showing hierarchical clustering of differentially expressed genes (rows) in heterozygous *AKAP11*-KO and WT samples. The expression levels across samples were standardized by Z-Score method. **D**) List of the top 30 downregulated and upregulated DEGs in heterozygous *AKAP11*-KO vs. WT. **E**) Over-representation analysis (ORA) of all DEGs, both up- and downregulated, based on Curated. Reactome database using ShinyGO0.77; FDR < 0.05. The background genes used were all the 23,590 genes that were considered expressed (see Methods). Shown here are the top 20 pathways. For the full list refer to Supplementary Figure 2A. **F**) GSEA showing enrichment of GO (molecular function) terms in upregulated and downregulated genes from heterozygous *AKAP11*-KO vs. WT comparison; Padj<0.05. Shown here are the top 10 pathways. For the full list refer to Supplementary Table 2. The size of the circles represents gene count (count of core enrichment genes); the colors represent the strength of -log (adjusted p-value), with red showing the most significant adjusted p-value, and gene ratio represents (count of core enrichment genes) / (count of pathway genes).

Genome-wide DMR profiling of heterozygous *AKAP11*-KO neurons compared to WT counterparts

We next performed WGBS using the three heterozygous *AKAP11*-KO clones and the three WT counterpart replicates and analyzed the genome-wide CpG DNA methylation modifications resulting from heterozygous *AKAP11*-KO. We detected the genome-wide DMRs (methylation values and p-values were averaged within each DMR), annotated them using Homer[47] (DMRs = Peaks), and identified the genes associated with them (referred to as DMR-associated genes). We found 813 total DMRs and 705 total DMR-associated genes in heterozygous *AKAP11*-KO compared to WT —some genes have multiple DMRs of both directions of changes (Supplementary Table 3). Our data indicates that, overall, the methylation differences within the DMRs of heterozygous *AKAP11*-KO vs. WT are relatively small in magnitude, which is consistent with the notion of DNA methylation being a more stable epigenetic mark, that tends to remain more intact once it is established, especially in differentiated cells[60]. Among these DNA methylation modifications in DMRs, we note that heterozygous knockout of *AKAP11* leads to more hypermethylated DMRs than hypomethylated ones (638 vs. 175, respectively; Figure 3A). The hierarchical clustering and heatmap of DMRs, based on the mean methylation level β value in 3 heterozygous *AKAP11*-KO and 3 WT replicates, distinguishes the large fraction of DMRs with elevated methylation status from the smaller group with decreased methylation status in heterozygous *AKAP11*-KO vs. WT. Labeled on the heatmap are the top 10 hyper- and hypo-methylated DMR-associated genes. These include genes with various roles in brain development, neural regulation, and function, including transcription factors (*OTX1*, *OTX2*, *NR2E1*, *IRX2*, and *PAX7*), neurotransmission and signaling (*ENPP2*, *GNG11*, *GREB1L*, *NAALADL2*), and other regulatory molecules and structural components (Figure 3B, Supplementary Figure 3A). The majority of DMRs resulting from heterozygous *AKAP11*-KO fall within the non-coding intergenic and intronic regions, suggesting their potential involvement in non-promoter transcription regulation (Figure 3C, Supplementary Figure 3B).

Subsequently, in search for over-represented pathways among all DMR-associated genes in heterozygous *AKAP11*-KO vs. WT, regardless of their direction of change, we performed ORA using Curated.Reactome database. We detected that the DMRs are primarily enriched in terms such as Class A/1 Rhodopsin–like receptors, peptide ligand-binding receptors, GPCR ligand binding, and GPCR downstream signaling (Figure 3D, Supplementary Figure 3C). Interestingly, the dysregulation of the GPCR-related signaling pathway in heterozygous *AKAP11*-KO obtained from the ORA of DMRs is in line with our findings from the ORA of DEGs. Lastly, using all these DMR-associated genes that were correlated with differential gene expression changes (59 genes; DEGs: P-adj < 0.05 & |log2FC| > 0.25), we performed GO molecular function enrichment analysis to uncover biological meaningful roles of specifically those DMR-associated genes that are linked with gene expression changes. The top 10 enriched GO terms highlight DNA-binding transcription factor activity (Figure 3E, Supplementary Figure 3D, Supplementary Table 4). While global DMR-associated genes were enriched in GPCR binding and signaling terms, those that were significantly linked with the gene expression modifications highlighted the enrichment of DNA binding transcription factor activity.

Overall, we show that in heterozygous *AKAP11*-KO compared to WT, the methylation difference values of the DMRs are quite subtle in magnitude, there is a higher number of hypermethylated DMRs than hypomethylated ones, and the DMRs are mainly residing within the intergenic and intronic regions. We also show that the global DMR-associated genes are enriched in pathways related to GPCRs' function and binding, while those that are specifically associated with differential gene expression modifications primarily function as DNA-binding transcription factors.

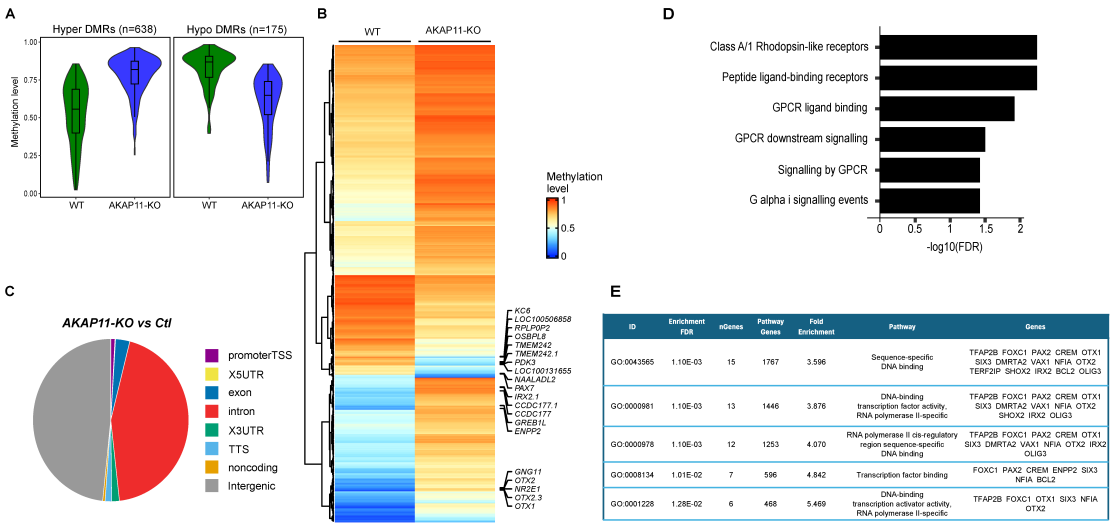

ID	Enrichment FDR	nGenes	Pathway Genes	Fold Enrichment	Pathway	Genes
GO:0043565	1.10E-03	15	1767	3.596	Sequence-specific DNA binding	TFAP2B FOXC1 PAX2 CREM OTX1 SIX3 DMRTA2 VAX1 NFIA OTX2 TERF2IP SHOX2 IRX2 BCL2 OLIG3
GO:0000981	1.10E-03	13	1446	3.876	DNA-binding transcription factor activity, RNA polymerase II-specific	TFAP2B FOXC1 PAX2 CREM OTX1 SIX3 DMRTA2 VAX1 NFIA OTX2 SHOX2 IRX2 OLIG3
GO:0000978	1.10E-03	12	1253	4.070	RNA polymerase II cis-regulatory region sequence-specific DNA binding	TFAP2B FOXC1 PAX2 CREM OTX1 SIX3 DMRTA2 VAX1 NFIA OTX2 IRX2 OLIG3
GO:0008134	1.01E-02	7	596	4.842	Transcription factor binding	FOXC1 PAX2 CREM ENPP2 SIX3 NFIA BCL2
GO:0001228	1.28E-02	6	468	5.469	DNA-binding transcription activator activity, RNA polymerase II-specific	TFAP2B FOXC1 OTX1 SIX3 NFIA OTX2

Figure 3. DMRs profiling of heterozygous *AKAP11*-KO compared to WT human iPSC-derived neurons. A) Violin plot for the overall distribution of methylation levels of hyper- and hypo-DMRs in heterozygous *AKAP11*-KO (colored blue) and WT (colored green) conditions (see Supplementary Table 3 for complete the list of DMRs). Methylation levels in WT and KO were obtained from the same hyper- or hypo-DMRs. Hypermethylation= positive methylation difference, Hypomethylation = negative methylation difference. **B**) Heatmap of patterns of methylation constructed using unsupervised hierarchical clustering of all DMRs identified (rows); columns represent the average of 3 WT reps and 3 KO clones. Orange and blue colors show the highest and lowest methylation levels, respectively. **C**) Pie chart of genomic distribution of 813 DMRs across the genome, illustrating the proportions of genomic features. **D**) Enrichment analysis (ORA) of all genome-wide DMRs, regardless of their direction of change, using Curated.Reactome databases. Generated using ShinyGO0.77; FDR < 0.05; top 20 pathways. **E**) Enrichment analysis (ORA) of genome-wide DMRs that are associated with gene expression changes (regardless of their direction; P-adj < 0.05 & |log2FC| > 0.25), using GO molecular function database. Generated using ShinyGO0.77; FDR < 0.05; top 5 pathways (redundancy removed). For the full top 20 pathways refer to Supplementary Figure 3D.

Enhancer activity dysregulations following heterozygous *AKAP11*-KO play a key role in the aberrant expression of neighboring genes

Based on our results described above that highlighted aberrant expression of genes related to transcription factor activity, as well as predominant distribution of DMRs in intergenic and intronic regions, we inferred potential dysregulation of transcription factor binding activity at cis-regulatory regions—mainly enhancers that play a role in aberrant gene regulatory networks. To test this hypothesis, we performed ChIP-seq for H3K27ac, marker of active enhancers[61-63], and investigated the modifications in heterozygous *AKAP11*-KO. Our data show that H3K27ac peaks with decreased intensities in heterozygous *AKAP11*-KO are preferentially located in intergenic regions while those with increased intensity present a more similar distribution to the set of all consensus peaks, with a relatively higher distribution in intronic regions (Figure 4A). Overall, in the intergenic regions, the number of H3K27ac differential peaks with reduced intensities in heterozygous *AKAP11*-KO was almost twice the number of differential peaks with increased intensities (6,763 down and 3,612 up; differential peaks at adj-P < 0.05 & |log2FC| > 1; Figure 4B). In the intronic regions, however, the difference between the number of increased and decreased differential peaks is less pronounced, yet more differential peaks show increased intensities in these regions (5719 down and 6146 up; Figure 4B).

Using heatmaps, we next separately profiled the intergenic and intronic H3K27ac enrichment patterns in heterozygous *AKAP11*-KO and WT centered at the center of the peaks, ±2 kb flanking region (signal from KO clones and WT replicates were averaged using WiggleTools[64]). Data were normalized so that each value represents the read count per base pair per 10 million reads. The heatmaps not only indicate a clear distinction between the enrichment of H3K27ac signals between heterozygous *AKAP11*-KO and WT in intergenic and intronic regions but also confirm the higher enrichment of intergenic H3K27ac peaks with differentially decreased intensities (down) and intronic peaks with differentially increased intensities (up) in heterozygous *AKAP11*-KO (Figure 4C and D; Supplementary Figure 4A-D). As H3K27ac marks active enhancers and active chromatin[61-63], and is indicative of enhancer activity[65], we utilized this chromatin signature to detect active enhancers and predict their target genes by linking the H3K27ac peaks with the nearest TSS of known genes. Acknowledging that the nearest assigned gene to the enhancer might not necessarily be the true target of that enhancer and that these enhancers might not be the main determinant of the gene expression fate of the target genes, we investigated the correlation between differential H3K27ac peaks changes (P < 0.05 & |log2FC| > 1) and differential gene expression modifications (adj-P < 0.05 & |log2FC| > 0.25) in intergenic and intronic regions. We found a significant positive correlation in both cases (intergenic: r = 0.57, p = 1e−41; intronic: r = 0.68, p = 3.7e−130; Figure 4E and H, Supplementary Table 5). To determine which set of target genes are mainly affected by the enhancers in our system, and as we already unraveled that enhancers with differentially decreased strength in heterozygous *AKAP11*-KO were preferentially mapped to intergenic regions and those with differentially increased intensities were more abundant in intronic regions, we narrowed down our focus to two groups of enhancers: 1. Group A (intergenic differential H3K27ac down, differential expression down; 105 genes): Intergenic

enhancers with decreased differential activity in heterozygous *AKAP11*-KO whose target genes show a negative differential gene expression fold change (Figure 4E), 2. Group B (intronic differential H3K27ac up, differential expression up; 242 genes): Intronic enhancers with increased differential activity in heterozygous *AKAP11*-KO whose target genes show a positive differential gene expression fold change (Figure 4H). To identify the functional properties of target genes within these two groups, we performed ORA using the GO molecular function database. For group A, the top GO terms were primarily related to DNA-binding transcription factor activity, highlighting that reduced intergenic enhancer activity upon heterozygous knockout of *AKAP11*, at least partially, accounts for the downregulation of genes involved in regulatory networks that play key roles as transcription factors or co-factors, as previously observed in our gene expression and DMR analysis (Figure 4F, Supplementary Figure 4E). The top GO terms in this group also include glycine transmembrane transporter activity (*SLC32A1* and *SLC6A5*), solute:cation symporter activity (*SLC32A1*, *SLC5A7*, *SLC10A2*, *SLC6A5*), and G protein-coupled receptor activity (*ADGRF5*, *ADCYAP1R1*, *HRH3* , *FZD10*, *CXCR4*, *SSTR1*, *GPRC5C*; Figure 4F, Supplementary Figure 4E). For group B the top GO terms involve signaling receptor binding, cytokine receptor binding, actin binding, high-density lipoprotein particle binding, frizzled binding, and structural constituent of cytoskeleton, among others (Figure 4F, Supplementary Figure 4F).

In order to detect the transcription factor binding motifs involved in the down- and upregulation of the genes enriched in GO terms (Group A and B), we performed transcription factor binding site (TFBS) motif analysis using HOMER[47]. Scanning the H3K27ac differential peaks (adj-P < 0.05 & |log2FC| > 1) that were associated with differential gene expression (adj-P < 0.05 & |log2FC| > 0.25) in the concordant direction for known TFBS motifs, we detected the most significant enrichment to be PBX2/Homer in group A (p=1e-3, 15.43% of target peaks, 7.70% of background) and NF1/Homer in group B (p=1e-5, 7.59% of target peaks, 3.53% of background).

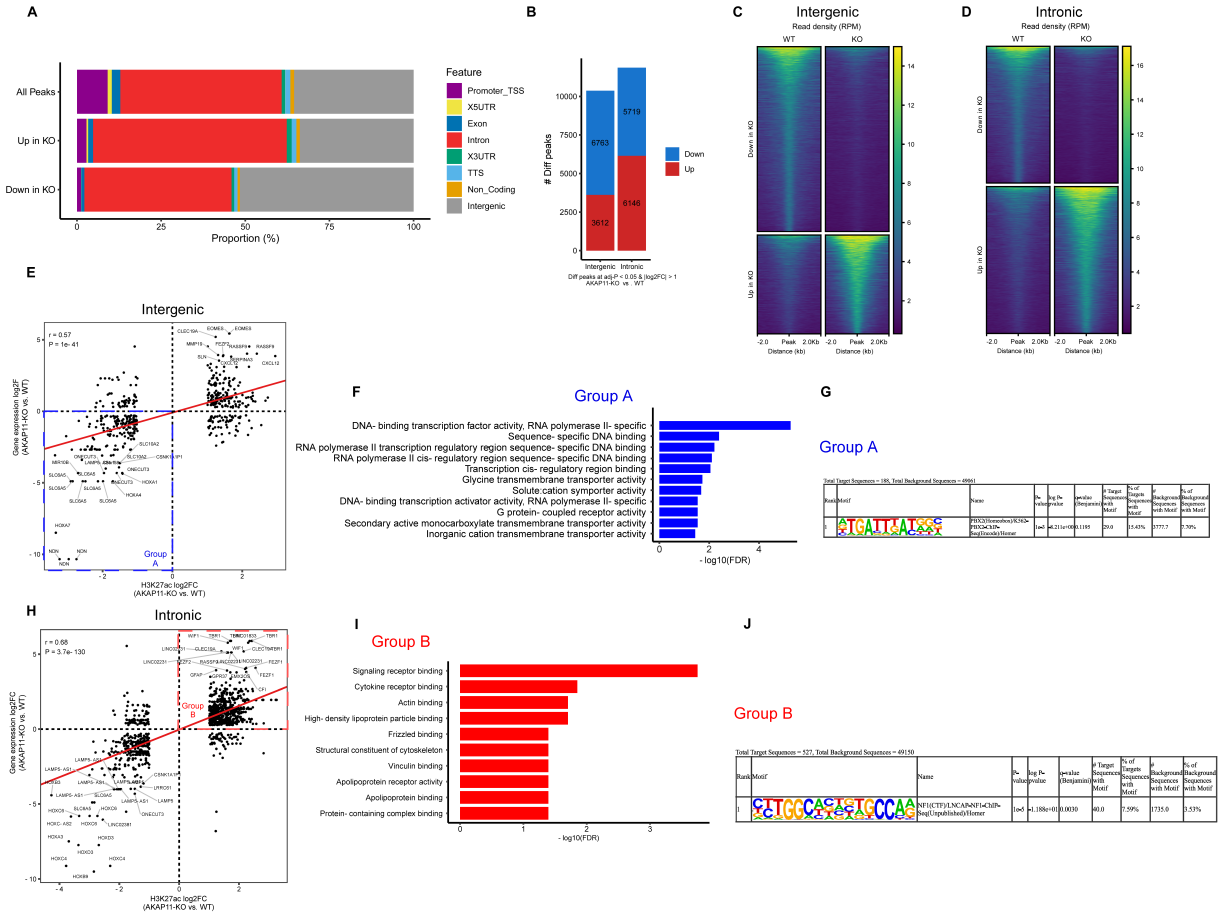

Figure 4. Intergenic and Intronic differential H3K27ac peaks profiling and investigating the association between H3K27ac level modifications and gene expression changes of target genes. A) Distribution of genomic compartments overlapping different subsets of H3K27ac peaks categorized by differential binding status; All peaks= all consensus peaks; Up in KO: differential H3K27ac peaks with increased intensities in heterozygous *AKAP11*-KO vs. WT; Down in KO: differential H3K27ac peaks with reduced intensities in heterozygous *AKAP11*-KO vs. WT. **B)** Number of differential H3K27ac peaks with increased (up) and decreased (down) intensities in heterozygous *AKAP11*-KO vs. WT; adj-P < 0.05 & |log2FC| > 1. **C, D)** Heatmap of intergenic and intronic differential H3K27ac signal enrichment (heterozygous *AKAP11*-KO and WT) centered at the center of peaks, ±2 kb flanking region. Rank ordered by intensity of H3K27ac peaks based on reads per million mapped reads (RPM). For the heat map of individual samples and average read density profiles refer to Supplementary Figure 4A-D. **E)** Correlation plot of differential gene expression fold changes (adj-P < 0.05 & |log2FC| > 0.25) and differential intergenic H3K27ac fold changes (adj-P < 0.05 & |log2FC| > 1), using a 100 kb distance cutoff. r = 0.57, p = 1e−41. **F)** GO-Molecular Function ORA of reduced intergenic H3K27ac peak intensities associated with decreased gene expression of target genes in heterozygous *AKAP11*-KO vs. WT (intergenic H3K27ac down, expression down: group A. Generated using ShinyGO-0.77; FDR < 0.05; top 20 pathways demonstrated (redundant terms removed). For the full top 20 list refer to Supplementary Figure 4E. **G)** Top

transcription factor binding sites query result for group A, using HOMER motif analysis (Known Motif Enrichment). Total Target Sequences = 188, Total Background Sequences = 49061. p= 1e-3. For the full table refer to Supplementary Table 6. **H)** Correlation plot of differential gene expression fold changes (adj-P < 0.05 & |log2FC| > 0.25) and differential intronic H3K27ac fold changes (adj-P < 0.05 & |log2FC| > 1), using a 100 kb distance cutoff. r = 0.68, p = 3.7e−130. **I)** GO-Molecular Function ORA of increased intronic H3K27ac peak intensities associated with increased gene expression of target genes in heterozygous *AKAP11*-KO vs. WT (intronic H3K27ac up, expression up: group B). Generated using ShinyGO-0.77; FDR < 0.05; top 20 pathways demonstrated. **J)** Top transcription factor binding site query result for group B, using HOMER motif analysis (Known Motif Enrichment). Total Target Sequences = 527, Total Background Sequences = 49150. p=1e-5. For the full table refer to Supplementary Table 6.

Intergenic and intronic differential enhancer activity is negatively correlated with methylation difference within DMRs in the respective enhancer regions in heterozygous *AKAP11*-KO vs. WT

To comprehensively explore the interplay between both intergenic and intronic enhancer activity, marked by H3K27ac, and alterations in DNA methylation levels at those regions, following the heterozygous knockout of *AKAP11* , correlation plots were constructed separately for intergenic and intronic regions, depicting the relationship between the differential H3K27ac log2FC (heterozygous *AKAP11*-KO vs. WT, adj-P < 0.05 & |log2FC| > 1) and methylation differences within the DMRs. Notably, we identified significant negative correlations between the subtle methylation differences in DMRs and differential H3K27ac changes in both intergenic and intronic regions ($r = -0.52$, $P = 0.00022$ and $r = -0.37$, $P = 0.019$, respectively; Figure 5A and B, Supplementary Table 7). This observation aligns with the established pattern where activated enhancers typically display a distinct reduction in DNA methylation (5mC), a phenomenon observed across various tissues and cell types[68-71].

Employing a multi-omics approach, we leveraged data on DEGs (cutoff: adj-P < 0.05 & |log2FC| > 1), DMRs (called as previously described in methods), and differential H3K27ac (cutoff: adj-P < 0.05 & |log2FC| > 1) to pinpoint the most profoundly impacted intergenic and intronic regulatory regions influenced by heterozygous LoF mutations in *AKAP11* . Given the overall negative correlation between DMR methylation differences and differential H3K27ac fold changes in our system, along with previous findings suggesting that transcription factor binding at methylated regions is linked with a reduction in DNA methylation, at least in a subtype of enhancers[68,72], we focused on differential enhancers exhibiting an inverse relationship with DMRs and concurrent differential expression of target genes. This analysis revealed that, in heterozygous *AKAP11*-KO, aberrantly methylated regions in intronic and intergenic enhancers with differential activity and an inverse direction of change significantly affected 3 regions that were linked to concordant gene expression alterations in the neighboring genes. These enhancers, tied with chromatin state changes and gene expression regulation of target genes, were mapped to Iroquois Homeobox 2 (*IRX2)*, C-type lectin domain containing 19A (*CLEC19A)*, and KN Motif And Ankyrin Repeat Domains 1 (*KANK1;* Figure 5E).

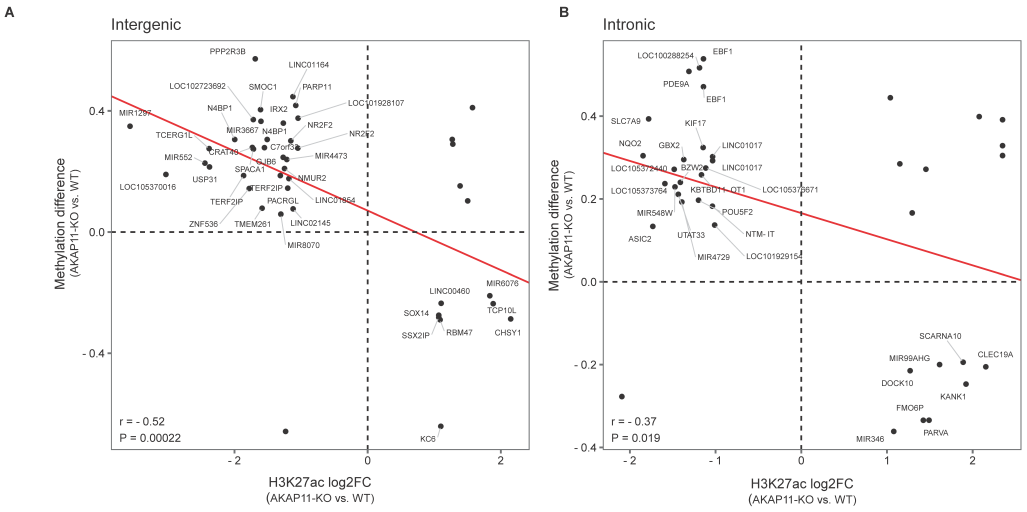

C

H3K27ac_Peak	DMR	Gene	Annotation	H3K27ac_ log2FC	H3K27ac_ Padj	Expression_ log2FC	Expression_ Padj	Methylation_ Difference	Methylation_ FDR	H3K27ac, Gene expression, and DNA methylation Trend
chr5_2741902_2745969	chr5_2744467_2745346	IRX2	Intergenic	-1.268	6.58E-06	-1.87144	4.85E-04	0.35952	4.76E-04	H3K27ac down |Expression down | Methylation up
chr16_19237297_19240735	chr16_19239562_19239705	CLEC19A	intron	2.152	1.38E-05	5.20109	3.87E-03	-0.20520	4.23E-03	H3K27ac up | Expression up | Methylation down
chr9_691631_701899	chr9_700398_700560	KANK1	intron	1.921	2.82E-08	2.01490	5.03E-03	-0.24700	2.70E-04	H3K27ac up | Expression up | Methylation down

Figure 5. DMR status in enhancers with concordant changes in the gene expression of target genes (using H3K27ac, DNA methylation, and gene expression datasets). A, B) Correlation plots of differential H3K27ac log2FC (adj-P < 0.05 & |log2FC| > 1) and methylation difference within DMRs for *AKAP11*-KO vs. WT in intergenic (r = −0.52, P = 0.00022) and intronic regions (r = −0.37, P = 0.019). **C**) A small subset of enhancers with differential activity with concordant differentially expressed target genes in *AKAP11*-KO showing significant negative correlation with DMRs at those enhancers. H3K27ac and Gene expression cutoffs: adj-P < 0.05 & |log2FC| > 1; DMR: callDMR at default parameters with a minimum length of 50 base pairs and 3 CpG sites.

Discussion

Given the complex polygenic nature of BD and SCZ, as well as our limited understanding of their origins and etiology, it is important to study novel risk genes. Genetic studies identified AKAP11 LoF as a candidate predisposing gene for both diseases. A study looking at AKAP11 mutant mice found that their EEG patterns resembled those observed in individuals with SCZ[31]. In another study, proteomic profiling of synapses found shared molecular pathway modifications between patients with SCZ, BD, and *AKAP11*-mutant mouse models--mainly pathways related to ribosomes, mitochondrial respiration, and vesicle trafficking pathways[34]. Our study, for the first time, uncovers the transcriptomic and epigenomic consequences of heterozygous LoF mutations in *AKAP11*, a novel rare-variant large-effect risk gene for BD and SCZ, in the context of human iPSC-derived neurons.

AKAP11 can modulate gene expression by influencing the activity of transcription factors through its role in PKA signaling. PKA has been implicated in a multitude of signaling processes and has an extensive array of downstream targets and processes[76] such as phosphorylating transcription factors (e.g. CREB), neurotransmitter receptors (e.g., AMPA receptors), cytoskeleton-associated proteins, ion channels, and elements of other signaling cascades[77,78]. Interestingly, our transcriptomic analysis found dysregulation of genes involved in many of these functions in our heterozygous *AKAP11*-KO neuronal model. Heterozygous LoF mutations in *AKAP11* may lead to reduced PKA activity[79] and as PKA regulates transcription factors, directly, or indirectly through binding to other kinases and substrates, its reduced activity could potentially lead to impaired activation of certain transcription factors and thus reduced expression of numerous genes that can themselves function as transcription factors or co-factors, as highlighted by our results. Particularly, in the case of CREB, its downstream target genes are involved in various processes, including metabolism (e.g., cytochrome c, *PEPCK*, and *aminolevulinate synthase*), transcription (e.g., *ATF-3*, *STAT3*, and *c-fos*), cell survival (e.g., *bcl-2*, *cyclin D1*, and c*yclin A*), and growth factors (e.g., *BDNF* and *FGF6*). CREB alone can regulate more than 4,000 genes[24,80], many of which are themselves transcription factors (e.g., *NF-IL6*, *ZNF268*, and *NR4A2*)[81]. Considering that phosphorylation of transcription factors can positively or negatively affect their activity[82], the wide range of genes with significantly up-or down-regulated profiles with their diverse roles in neurons could be a direct or indirect result of aberrant PKA-dependant phosphorylation of transcription factors.

Our findings also suggest that the downregulation of genes involved in DNA-binding transcription factor activity can be partly explained by the reduced activity of their intergenic enhancers, which indicates the involvement of histone acetyltransferases (HATs) and/or HDACs and chromatin accessibility changes at such regulatory regions. The acetylation and deacetylation of histones, facilitated by HATs and HDACs, respectively, play a role in regulating gene transcription[73,83,84]. It has been shown that the AKAP11-involved cAMP/PKA signaling inhibits gene transcription by phosphorylating HDACs, such as HDAC5, and preventing their export from the nucleus[25]. In addition, AKAP11-PP1 complex can affect HDAC6 stability[85]. Moreover, AKAP11-PKA-regulated GSK3B, one of the molecular targets of lithium, which is the most common medication to prevent recurrences of both manic and depressive episodes in BD patients[18-21], has been suggested to be involved in the regulation of HDAC6 activity through phosphorylation events[26]

. On the other hand, CREB binding protein (CREBBP), which is the transcriptional coactivator of CREB and is also phosphorylated by PKA, can function as an intrinsic HAT[86,87]. The DMR-associated genes that overlap with gene expression modifications in heterozygous *AKAP11*-KO also refer to transcription factor activity as the top GO term, suggesting that DMRs play partial roles in such gene expression dysregulations in heterozygous *AKAP11*-KO.

Consistent with previous research providing evidence of downregulated mitochondrial ribosomal subunit genes in the brain and blood samples of SCZ patients[88] as well as decreased synaptic mitochondrial content and ribosomal proteins in patients with BD, SCZ, and *AKAP11*-mutant mice[34], we detected significant downregulation of ribosomal protein genes and mitochondrial ribosomal protein genes along with other regulators involved in protein synthesis in our model. One possible explanation for the decreased expression of ribosomal proteins following heterozygous KO of *AKAP11* could be the inhibition of mTORC1 upon modifications in the upstream signals including growth factors, stress, or energy status[89]. Mitochondrial ribosomal proteins, particularly, are involved in mitochondrial oxidative phosphorylation (OXPHOS)[90]. It has been reported that the absence of *AKAP11* interrupts mitochondrial respiration by blocking the PKA activity[79]. Furthermore, synaptic mitochondria content supplies energy for local translation in the process of synaptic plasticity[91,92]. As ribosomal proteins are predominantly located in neurites, downregulation of ribosomal protein genes may lead to reduced synthesis of synaptic proteins[93] as a part of a plasticity mechanism where neurons adjust their excitability in response to network activity[93], an event that occurs in neuropsychiatric disorders[94,95].

We found that heterozygous knockout of *AKAP11 led to* upregulation of pathways such as actin-binding, calcium ion binding, SH3 domain binding, lipid binding, and PDZ domain binding, which include genes involved in cell adhesion, motility, ECM interactions, or cytoskeletal integrity--pathways that have been previously suggested to be associated with lithium response[96,97]. Moreover, we found that the upregulated genes that were linked to increased intronic enhancer activity were primarily enriched in similar pathways suggesting that intronic enhancer activity through HATs and/or HDACs, plays a role, at least in part, in such dysregulations. It is known that generally, IQ domain GTPase-activating proteins (IQGAPs) play a role in remodeling the cytoskeleton, cell-cell adhesion, and regulating cell growth[22,98,99]. Functional studies have reported that *AKAP11* and the cytoskeletal scaffolding proteins IQGAP1/2 interactions affect cell motility[100] and actin cytoskeleton[22]. In addition, *AKAP11* inhibits GSK3B, and GSK3, through its substrates, can regulate actin, tubulin, and the cytoskeleton structure[100]. All these findings support the involvement of *AKAP11* in the regulation of cell motility and actin cytoskeleton possibly through interacting with GSK3 and IQGAPs, which may account for the transcriptomic aberrations seen in the knockout of *AKAP11*. ECM dysregulations and decreased actin-related gene expression have been reported in the post-mortem cortex studies of SCZ patients[101,102]. Impaired adhesion is closely connected to both cell migration and axon guidance, pathways that exhibit abnormalities in genes associated with the risk of SCZ[103-105]. Additionally, there is a BD and SCZ-specific association observed in pathways related to the dynamic regulation and restructuring of cytoskeletal actin[106,107], cytoskeletal proteins[108], and cellular communication with ECM[109]. Lastly, our GSEA results highlight cytokine activity upregulation in heterozygous *AKAP11*-KO and the follow-up analysis of upregulated genes associated with significantly increased

intronic enhancer activity suggests that enhancer activity alterations and potential involvement of histone HATs and/or HDACs partially explain the dysregulation of transcription of the genes involved in cytokine receptor binding. Cytokine activity in the brain can affect mood, memory, cognition, and sleep and modulate neuroendocrine stress responses[110]. Notably, literature evidence highlights a potential causative role for cytokines in SCZ development[111] as well as a partial overlap in the increased blood cytokine levels in patients with BD with psychotic symptoms and first-episode SCZ[112]. Most importantly, dysregulated blood levels of cytokine network elements have been detected in BD, SCZ, and major depressive disorder [113-119].

Non-promoter regulatory elements are rich in factors that contribute to neuropsychiatric heritability[120-122]. It has been demonstrated that the levels of DNA methylation, H3K27ac, and overall chromatin accessibility in these areas can have effects on disorders specific to certain regions of the brain[120-122]. Moreover, numerous genetic risk loci associated with SCZ and BD have been previously reported to be within non-coding regions, including introns, intergenic regions, and noncoding RNA genes, indicating the pivotal involvement of gene regulation in the disease's development[73-75]. Most importantly, BD and SCZ brains have previously demonstrated dysregulation of regulatory sequences, particularly modifications that affect the neuronal H3K27ac levels[123]. Our findings from intergenic and intronic H3K27ac motif analysis show that, in heterozygous *AKAP11*-KO, the intergenic enhancers with reduced transcription factor binding activity that were linked to downregulation of target genes were mainly enriched in PBX2 binding motifs, suggesting a potential impairment of PBX2 transcription factor binding at intergenic enhancers and subsequent downregulation of target genes. *PBX2* (HOX12) encodes a widely expressed member of the TALE/PBX homeobox family and interacts with a specific group of HOX proteins, improving their capacities for DNA binding in terms of both affinities and specificities[124,125]. Genome-wide association studies have reported strong associations of PBX2 with the risk of SCZ and autism spectrum[126,127]. On the other hand, intronic enhancers with elevated transcription factor binding activity, linked with the upregulation of target genes, were significantly enriched in NF1 binding motifs, suggesting a potential role of NF1 binding at intronic enhancers in the upregulation of target genes. NF1 transcription factors can bind to specific DNA sequences with high affinity and are abundant in cerebellar granule neurons[128,129]. Their activity can be modulated post-transcriptionally, through phosphorylation[130-132] or regulation of mRNA stability[130,133]. The DNA binding capability of a particular form of NF1 has been demonstrated to be dependent on ECM in mammary epithelial cells[134].

Investigating the genome-wide DNA methylation modifications not only uncovered the overall genome-wide changes seen with the knockout of *AKAP11* but also, along with the transcriptomic data, showed that the DMRs were specifically linked to gene expression dysregulations. Such DMR-associated genes were primarily involved in transcription factor binding functions. Although DMR-associated genes showed enrichment of GPCR-related functions, further investigation found that DMRs did not have a considerable effect on transcription dysregulation of genes involved in GPCR-related functions. Our findings imply that a portion of GPCR-signaling-related gene expression modifications, notably *GPRC5C*, *FZD10*, and *WNT2B*, are associated with enhancer activity alterations, suggesting the potential involvement of HATs and/or HDACs. Altered G-protein-linked signaling system and its

downstream targets have been traditionally implicated in the pathophysiology and pharmacology of BD, SCZ, and major depressive disorder by our group and others[135-140]. The observed overall negative correlation between intronic and intergenic methylation differences in DMRs and differential H3K27ac changes in those regions suggests that, for the most part, transcription factor binding at active enhancers is inversely related to DNA methylation status in those sites. Previous findings reported that transcription factor binding at methylated regions is associated with decreased DNA methylation[68,72]. Notably, beyond preventing aberrant activation of the genome, a recent study showed that DNA methylation plays a direct role in regulating transcription factor binding in a small subset of cell type-specific active enhancers[72]. We detected enhancers with differential activity, overlapping DMRs of the opposite direction of change, which were linked to concordant differential gene expression changes to be mapped to *IRX2, CLEC19A*, and *KANK1*. Generally, IRX transcription factors play roles in neuronal function and development[141]. IRX2, a transcriptional inhibitor, has been suggested to have a connection to social behaviors in animals[142,143]. The expression of *IRX2* is known to be modulated by the three-dimensional structure of chromatin, which itself is controlled by the architectural protein known as CCCTC-binding factor (CTCF)[144-146]. Intergenic hypermethylation of *IRX2* noted by DMRs, along with a significant decrease in H3K27ac peaks in that region and its reduced gene expression level in heterozygous *AKAP11*-KO implies possible chromatin structure state changes and is in concordant with previous reports suggesting DNA methylation's ability to compete with CTCF binding, particularly at CpGs in key regulatory regions[147,148]. KANK1 plays a pivotal role in cell motility and cytoskeleton formation through modulating actin polymerization[149,150]. Its activity has been shown to inhibit actin fiber formation, cell migration, RhoA activity, and neurite outgrowth[151]. Interestingly, the first large-scale meta-analysis of CNVs across SCZ, bipolar disease, depression, ADHD, and autism cohorts has detected enrichment of duplications in *KANK1* in all five groups[152]. Finally, CLEC19A, which belongs to the C-type lectin family, is highly expressed in brain tissue[152]. The *CLEC19A* gene is close to a locus that has been previously associated with attention deficit hyperactivity disorder (ADHD)[153] and it has been suggested that there is common genetic etiology between ADHD, BD, and SCZ [154].

Overall, our investigations shed light on the impact of heterozygous *AKAP11*-KO on gene expression modifications, particularly genes playing roles as DNA-binding transcription factors, actin and cytoskeleton regulators, and cytokine receptors, which are at least partially dysregulated by enhancer activity alterations, marked by H3K27ac, as well as DNA methylation modifications detected within DMRs. We also highlighted the enrichment of GPCR binding and signaling within DEGs, genome-wide DMR-associated genes, and showed that a portion of those DEGs were linked to enhancer activity alterations. Further investigation is essential to explore the precise mechanism of action and functional significance of heterozygous *AKAP11*-KO within the pathways, roles, and epigenetic regulators linked to such modifications. This is imperative for advancing our comprehension of the roots and etiology of BD and SCZ as well as eventually finding the most appropriate therapeutic agents for patients.

Supplementary Material

Supplementary Figures

Supplementary Figure 1

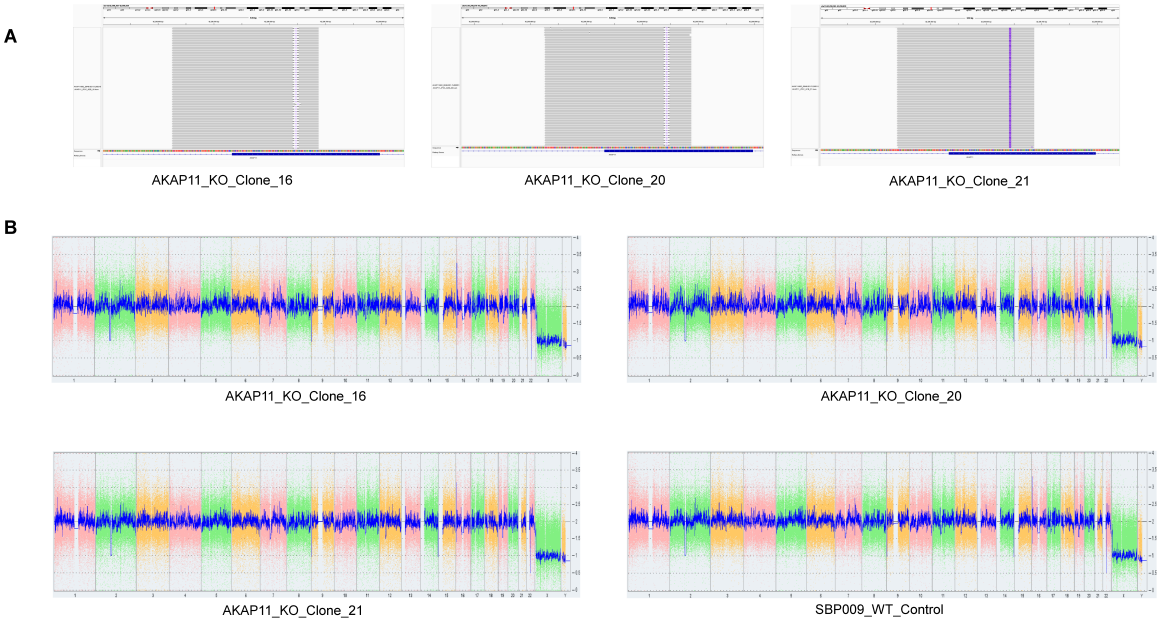

C

Samples	Neurons	Astrocytes	Oligodendrocytes	Microglia	Endothelia
AKAP11_KO_Clone_16	0.482	0.278	0.043	0.037	0.160
AKAP11_KO_Clone_20	0.702	0.121	0.041	0.045	0.091
AKAP11_KO_Clone_21	0.455	0.323	0.043	0.035	0.143
SBP009_WT_CTL_1	0.455	0.270	0.055	0.050	0.170
SBP009_WT_CTL_2	0.474	0.276	0.056	0.046	0.149
SBP009_WT_CTL_3	0.527	0.250	0.048	0.045	0.130

Supplementary Figure 1. Validation of *AKAP11* heterozygous knockout in three isogenic clones, their chromosomal integrity, and abundance of neurons in the cultures. A) Miseq amplicon sequencing results showing heterozygous frameshift LoF mutations in iPSC *AKAP11*-KO clones. **B**) KaryoStat+ assay for digitally visualizing chromosomal aberrations. The size of structural aberration detectable is > 1 Mb for chromosomal gains and losses. The smooth signal plot is the smoothing of the log2 ratios which show the signal intensities of probes on the microarrayCN = 2. A value of 3 represents chromosomal gain (CN = 3). A value of 1 represents a chromosomal loss (CN = 1). **C**) Cell type deconvolution using bulk RNA-seq data and dtangle method[51] from BrainDeconvShiny[155], showing different cell types present in the cultures.

Supplementary Figure 2

A

Enrichment FDR	nGenes	Pathway Genes	Fold Enrichment	Pathway	Genes
6.09E-04	27	454	2.830	GPCR ligand binding	UTS2 WNT8B VIPR2 CXCL12 CCKBR FZD10 PTGFR ADM2 MCHR1 NTS WNT2B ANXA1 HTR1B DHH SSTR1 CRH F2RL2 OXGR1 BDKRB2 GPR37 TRH S1PR5 OXTR CHRM2 CHRM5 NMB GRM3
6.09E-04	20	227	3.442	G alpha q signalling events	UTS2 CCKBR PTGFR ITPR2 MCHR1 NTS ANXA1 DGKB RGS3 RGS5 RGS16 EGFR PRKCA ABHD6 F2RL2 BDKRB2 TRH OXTR CHRM5 NMB
9.27E-04	11	73	5.577	Non-integrin membrane-ECM interactions	ACTN1 ITGA6 VTN LAMA4 FN1 LAMC1 PRKCA COL1A2 COL4A5 COL4A6 DMD
1.04E-03	42	1263	2.095	Signaling by GPCR	UTS2 WNT8B LRP2 VIPR2 CXCL12 CCKBR FZD10 PLA2G4A PTGFR ITPR2 ADM2 MCHR1 PDE11A NTS WNT2B ANXA1 HTR1B BCO1 DGKB RGS3 DHH SSTR1 RGS5 RGS16 EGFR CRH PRKCA ABHD6 ARHGEF3 F2RL2 OXGR1 BDKRB2 GPR37 TRH PDE7B S1PR5 OXTR CHRM2 GPC6 CHRM5 NMB GRM3
1.87E-03	24	418	2.688	Extracellular matrix organization	CDH1 ACTN1 P3H2 ITGA6 VTN LAMA4 FN1 TGFB3 MMP19 GDF5 ITGA7 LAMC1 LOXL4 ITGB7 ADAMTS16 HAPLN1 PRKCA COL1A2 HTRA1 PPIB COL22A1 COL4A5 COL4A6 DMD
3.25E-03	38	1199	2.049	GPCR downstream signalling	UTS2 LRP2 VIPR2 CXCL12 CCKBR PLA2G4A PTGFR ITPR2 ADM2 MCHR1 PDE11A NTS ANXA1 HTR1B BCO1 DGKB RGS3 SSTR1 RGS5 RGS16 EGFR CRH PRKCA ABHD6 ARHGEF3 F2RL2 OXGR1 BDKRB2 GPR37 TRH PDE7B S1PR5 OXTR CHRM2 GPC6 CHRM5 NMB GRM3
3.94E-03	19	321	2.895	Class A/1 Rhodopsin-like receptors	UTS2 CXCL12 CCKBR PTGFR MCHR1 NTS ANXA1 HTR1B SSTR1 F2RL2 OXGR1 BDKRB2 GPR37 TRH S1PR5 OXTR CHRM2 CHRM5 NMB
9.26E-03	13	188	3.485	Peptide ligand-binding receptors	UTS2 CXCL12 CCKBR MCHR1 NTS ANXA1 SSTR1 F2RL2 BDKRB2 GPR37 TRH OXTR NMB
1.21E-02	10	90	4.162	ECM proteoglycans	VTN LAMA4 FN1 TGFB3 ITGA7 LAMC1 HAPLN1 COL1A2 COL4A5 COL4A6
1.37E-02	6	122	6.971	Complement cascade	CD59 VTN SERPING1 COLEC10 PROS1 CFI
2.01E-02	6	34	6.435	Syndecan interactions	ACTN1 ITGA6 VTN FN1 PRKCA COL1A2
2.06E-02	4	10	11.154	ATF6 ATF6-alpha activates chaperone genes	HSPA5 HSP90B1 DDIT3 CALR
2.39E-02	12	136	3.127	Activation of anterior HOX genes in hindbrain development during early embryogen	HOXA1 HOXA2 HOXA3 HOXB3 HOXD3 HOXD4 HOXB2 HOXB4 H2AC7 HOXA4 HOXC4 H4C6
2.39E-02	12	136	3.127	Activation of HOX genes during differentiation	HOXA1 HOXA2 HOXA3 HOXB3 HOXD3 HOXD4 HOXB2 HOXB4 H2AC7 HOXA4 HOXC4 H4C6
2.39E-02	7	41	5.005	MET promotes cell motility	MET RAPGEF1 LAMA4 FN1 LAMC1 TNS3 COL1A2
2.39E-02	5	111	7.338	Reg. of Complement cascade	CD59 VTN SERPING1 PROS1 CFI
2.97E-02	6	55	5.577	Laminin interactions	ITGA6 LAMA4 ITGA7 LAMC1 COL4A5 COL4A6
3.06E-02	4	12	9.295	ATF6 ATF6-alpha activates chaperones	HSPA5 HSP90B1 DDIT3 CALR
3.09E-02	13	221	2.832	Biological oxidations	FMO1 FMO2 CYP26A1 CYP3A5 AHR CHAC1 GSTM1 GSTM5 CMBL GLYATL1 CYP4A11 CYP26C1 SULT1C2
4.47E-02	9	109	3.485	Integrin cell surface interactions	CDH1 ITGA6 VTN FN1 ITGA7 ITGB7 COL1A2 COL4A5 COL4A6
4.58E-02	20	470	2.137	G alpha i signalling events	LRP2 CXCL12 PLA2G4A ITPR2 MCHR1 ANXA1 HTR1B BCO1 RGS3 SSTR1 RGS5 RGS16 PRKCA OXGR1 BDKRB2 GPR37 S1PR5 CHRM2 GPC6 GRM3
4.58E-02	6	43	4.921	Bile acid and bile salt metabolism	OSBPL3 HSD3B7 ABCC3 SLC10A2 ACOX2 FABP6
4.58E-02	2	3	27.884	FMO oxidises nucleophiles	FMO1 FMO2
4.58E-02	2	3	27.884	Reg. of thyroid hormone activity	DIO3 DIO2

Supplementary Figure 2. Results table of ORA using all DEGs. **A**) Table of overrepresented Reactome pathways resulting from ORA of DEGs (both up- and downregulated) of heterozygous *AKAP11*-KO vs. WT. Generated using ShinyGO 0.77; FDR < 0.05; top 20 pathways demonstrated.

Supplementary Figure 3

A

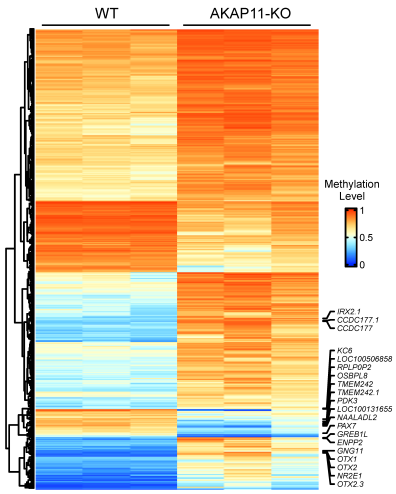

B

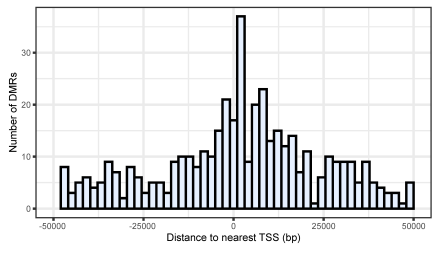

C

Enrichment FDR	nGenes	Pathway Genes	Fold Enrichment	Pathway	Genes
5.71E-03	18	321	3.297	Class A/1 Rhodopsin-like receptors	OPRK1 PROKR2 PDYN OPRM1 CNR1 CXCR4 NMUR2 CHRM3 ANXA1 EDNRB EDNRA CXCL13 RXFP1 DRD1 NPY2R HRH1 S1PR3 NPS
5.71E-03	13	188	4.139	Peptide ligand-binding receptors	PRK1 PROKR2 PDYN OPRM1 CXCR4 NMUR2 ANXA1 EDNRB EDNRA CXCL13 RXFP1 NPY2R NPS
1.20E-02	21	454	2.659	GPCR ligand binding	OPRK1 PROKR2 PDYN OPRM1 GNB4 CNR1 CXCR4 GNG11 NMUR2 CHRM3 ANXA1 EDNRB EDNRA CXCL13 SHH RXFP1 DRD1 NPY2R HRH1 S1PR3 NPS
3.14E-02	31	1199	2.023	GPCR downstream signalling	TRIO OPRK1 PROKR2 PDYN PRKAR1A OPRM1 GNB4 CNR1 CXCR4 OR2B6 GNG11 GNAI1 NMUR2 CHRM3 ANXA1 EDNRB RGS3 CAMKMT EDNRA PDE1C CXCL13 TIAM1 PLB1 OR2K2 RXFP1 PDE4B DRD1 NPY2R HRH1 S1PR3 NPS
3.74E-02	32	1263	1.933	Signaling by GPCR	TRIO OPRK1 PROKR2 PDYN PRKAR1A OPRM1 GNB4 CNR1 CXCR4 OR2B6 GNG11 GNAI1 NMUR2 CHRM3 ANXA1 EDNRB RGS3 CAMKMT EDNRA PDE1C CXCL13 TIAM1 PLB1 SHH OR2K2 RXFP1 PDE4B DRD1 NPY2R HRH1 S1PR3 NPS
3.74E-02	19	470	2.461	G alpha i signalling events	OPRK1 PDYN PRKAR1A OPRM1 GNB4 CNR1 CXCR4 GNG11 GNAI1 NMUR2 ANXA1 RGS3 CAMKMT PDE1C CXCL13 PLB1 PDE4B NPY2R S1PR3

D

ID	Enrichment FDR	nGenes	Pathway Genes	Fold Enrichment	Pathway	Genes
GO:0000978	1.10E-03	12	1253	4.070	RNA polymerase II cis-regulatory region sequence-specific DNA binding	TFAP2B FOXC1 PAX2 CREM OTX1 SIX3 DMRTA2 VAX1 NFIA OTX2 IRX2 OLIG3
GO:0000981	1.10E-03	13	1446	3.876	DNA-binding transcription factor activity, RNA polymerase II-specific	TFAP2B FOXC1 PAX2 CREM OTX1 SIX3 DMRTA2 VAX1 NFIA OTX2 SHOX2 IRX2 OLIG3
GO:0000987	1.10E-03	12	1272	3.996	Cis-regulatory region sequence-specific DNA binding	TFAP2B FOXC1 PAX2 CREM OTX1 SIX3 DMRTA2 VAX1 NFIA OTX2 IRX2 OLIG3
GO:0003700	1.10E-03	13	1515	3.738	DNA-binding transcription factor activity	TFAP2B FOXC1 PAX2 CREM OTX1 SIX3 DMRTA2 VAX1 NFIA OTX2 SHOX2 IRX2 OLIG3
GO:0043565	1.10E-03	15	1767	3.596	Sequence-specific DNA binding	TFAP2B FOXC1 PAX2 CREM OTX1 SIX3 DMRTA2 VAX1 NFIA OTX2 TERF2IP SHOX2 IRX2 BCL2 OLIG3
GO:1990837	2.58E-03	13	1660	3.337	Sequence-specific double-stranded DNA binding	TFAP2B FOXC1 PAX2 CREM OTX1 SIX3 DMRTA2 VAX1 NFIA OTX2 SHOX2 IRX2 OLIG3
GO:0003690	3.57E-03	13	1775	3.143	Double-stranded DNA binding	TFAP2B FOXC1 PAX2 CREM OTX1 SIX3 DMRTA2 VAX1 NFIA OTX2 SHOX2 IRX2 OLIG3
GO:0000976	4.51E-03	12	1596	3.220	Transcription cis-regulatory region binding	TFAP2B FOXC1 PAX2 CREM OTX1 SIX3 DMRTA2 VAX1 NFIA OTX2 IRX2 OLIG3
GO:0001067	4.51E-03	12	1598	3.215	Transcription regulatory region nucleic acid binding	TFAP2B FOXC1 PAX2 CREM OTX1 SIX3 DMRTA2 VAX1 NFIA OTX2 IRX2 OLIG3
GO:0008134	1.01E-02	7	596	4.842	Transcription factor binding	FOXC1 PAX2 CREM ENPP2 SIX3 NFIA BCL2
GO:0001228	1.28E-02	6	468	5.469	DNA-binding transcription activator activity, RNA polymerase II-specific	TFAP2B FOXC1 OTX1 SIX3 NFIA OTX2
GO:0001216	1.29E-02	6	474	5.381	DNA-binding transcription activator activity	TFAP2B FOXC1 OTX1 SIX3 NFIA OTX2
GO:0004167	4.21E-02	1	5	332.705	Dopachrome isomerase activity	DCT
GO:0004949	4.21E-02	1	3	332.705	Cannabinoid receptor activity	CNR1

Supplementary Figure 3. Heterozygous *AKAP11*-KO vs. WT DMR Characterization. A) Heatmap of patterns of methylation constructed using unsupervised hierarchical clustering of all DMRs identified (rows); columns represent the 3 WT replications and the 3 heterozygous *AKAP11*-KO clones. Orange and blue colors show the highest and lowest methylation levels, respectively. **B**) Histogram showing the locations of heterozygous *AKAP11*-KO vs. WT DMRs with respect to the closest TSS. TSS: transcription start site. **C**) Table of ORA of DMR-associated genes from heterozygous *AKAP11*-KO vs. WT comparison, using Curated.Reactome database in ShinyGO 0.77; pFDR < 0.05. The background genes used here were the same background gene list (23,590 genes that passed a low filter) from the RNA-Seq data. **D**) Table of top 20 GO molecular function terms (full list). ORA of genome-wide DMRs (regardless of their direction) that are associated with DEGs (regardless of their direction; at cutoff P-adj < 0.05 & |log2FC| > 0.25), regardless

of their direction of change, using GO molecular function databases. Generated using ShinyGO 0.77; FDR < 0.05; top 10 pathways with redundancy removed. The background genes used here were the same background gene list (23,590 genes) obtained from our RNA-seq analysis.

Supplementary Figure 4.

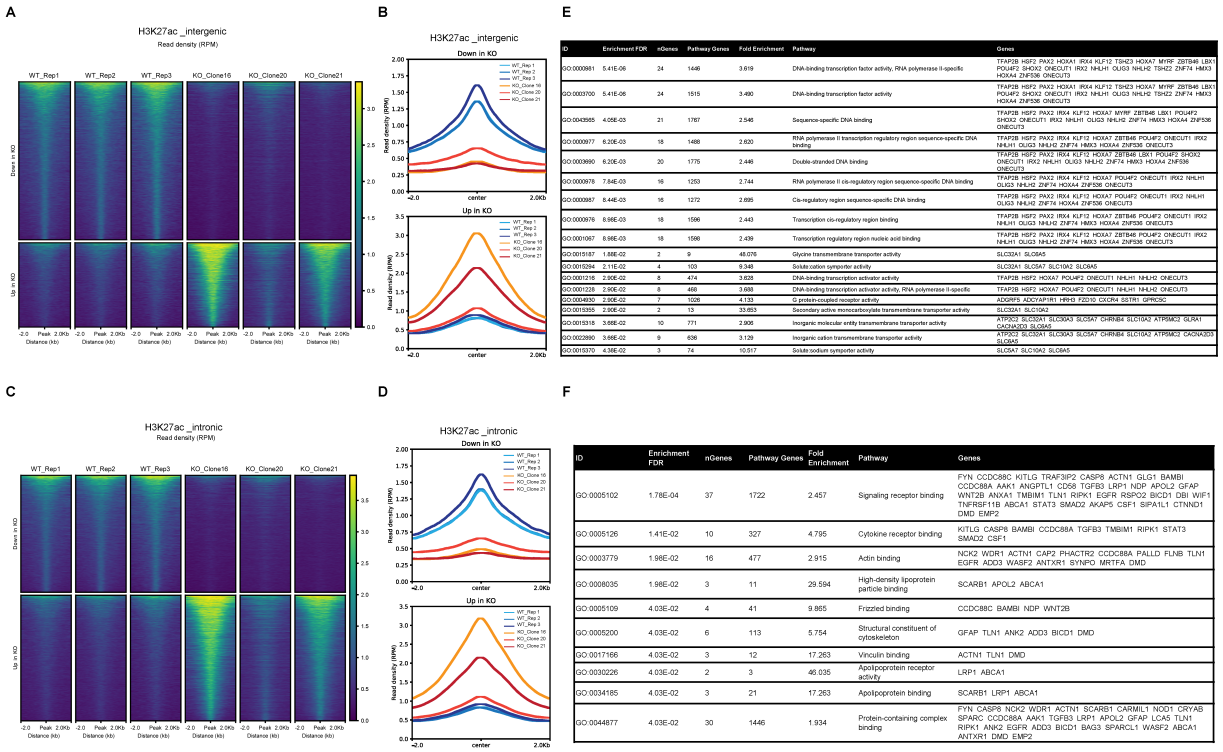

ID	Enrichment FDR	nGenes	Pathway Genes	Fold Enrichment	Pathway	Genes
GO:0000981	5.41E-06	24	1446	3.619	DNA-binding transcription factor activity, RNA polymerase II-specific	TFAP2B HSF2 PAX2 HOXA1 IRX4 KLF12 TSHZ3 HOXA7 MYRF ZBTB46 LBX1 POU4F2 SHOX2 ONECUT1 IRX2 NHLH1 OLIG3 NHLH2 TSHZ2 ZNF74 HMX3 HOXA4 ZNF536 ONECUT3
GO:0003700	5.41E-06	24	1515	3.490	DNA-binding transcription factor activity	TFAP2B HSF2 PAX2 HOXA1 IRX4 KLF12 TSHZ3 HOXA7 MYRF ZBTB46 LBX1 POU4F2 SHOX2 ONECUT1 IRX2 NHLH1 OLIG3 NHLH2 TSHZ2 ZNF74 HMX3 HOXA4 ZNF536 ONECUT3
GO:0043565	4.05E-03	21	1787	2.546	Sequence-specific DNA binding	TFAP2B HSF2 PAX2 IRX4 KLF12 HOXA7 MYRF ZBTB46 LBX1 POU4F2 SHOX2 ONECUT1 IRX2 NHLH1 OLIG3 NHLH2 ZNF74 HMX3 HOXA4 ZNF536 ONECUT3
GO:0000977	6.20E-03	18	1488	2.620	RNA polymerase II transcription regulatory region sequence-specific DNA binding	TFAP2B HSF2 PAX2 IRX4 KLF12 HOXA7 ZBTB46 POU4F2 ONECUT1 IRX2 NHLH1 OLIG3 NHLH2 ZNF74 HMX3 HOXA4 ZNF536 ONECUT3
GO:0003690	6.20E-03	20	1775	2.446	Double-stranded DNA binding	TFAP2B HSF2 PAX2 IRX4 KLF12 HOXA7 ZBTB46 LBX1 POU4F2 SHOX2 ONECUT1 IRX2 NHLH1 OLIG3 NHLH2 ZNF74 HMX3 HOXA4 ZNF536 ONECUT3
GO:0000978	7.84E-03	16	1253	2.744	RNA polymerase II cis-regulatory region sequence-specific DNA binding	TFAP2B HSF2 PAX2 IRX4 KLF12 HOXA7 POU4F2 ONECUT1 IRX2 NHLH1 OLIG3 NHLH2 ZNF74 HOXA4 ZNF536 ONECUT3
GO:0000987	8.44E-03	16	1272	2.695	Cis-regulatory region sequence-specific DNA binding	TFAP2B HSF2 PAX2 IRX4 KLF12 HOXA7 POU4F2 ONECUT1 IRX2 NHLH1 OLIG3 NHLH2 ZNF74 HOXA4 ZNF536 ONECUT3
GO:0000976	8.96E-03	18	1596	2.443	Transcription cis-regulatory region binding	TFAP2B HSF2 PAX2 IRX4 KLF12 HOXA7 ZBTB46 POU4F2 ONECUT1 IRX2 NHLH1 OLIG3 NHLH2 ZNF74 HMX3 HOXA4 ZNF536 ONECUT3
GO:0001067	8.96E-03	18	1598	2.439	Transcription regulatory region nucleic acid binding	TFAP2B HSF2 PAX2 IRX4 KLF12 HOXA7 ZBTB46 POU4F2 ONECUT1 IRX2 NHLH1 OLIG3 NHLH2 ZNF74 HMX3 HOXA4 ZNF536 ONECUT3
GO:0015187	1.58E-02	2	9	48.076	Glycine transmembrane transporter activity	SLC32A1 SLC6A5
GO:0015294	2.11E-02	4	103	9.348	Solute:cation symporter activity	SLC32A1 SLC5A7 SLC10A2 SLC6A5
GO:0001216	2.90E-02	8	474	3.628	DNA-binding transcription activator activity	TFAP2B HSF2 HOXA7 POU4F2 ONECUT1 NHLH1 NHLH2 ONECUT3
GO:0001228	2.90E-02	8	468	3.688	DNA-binding transcription activator activity, RNA polymerase II-specific	TFAP2B HSF2 HOXA7 POU4F2 ONECUT1 NHLH1 NHLH2 ONECUT3
GO:0004930	2.90E-02	7	1026	4.133	G protein-coupled receptor activity	ADGRF5 ADCYAP1R1 HRH3 FZD10 CXCR4 SSTR1 GPR35C
GO:0015295	2.90E-02	2	13	33.653	Secondary active monocarboxylate transmembrane transporter activity	SLC32A1 SLC10A2
GO:0015318	3.66E-02	10	771	2.906	Inorganic molecular entity transmembrane transporter activity	ATP2C2 SLC32A1 SLC30A3 SLC5A7 CHRNB4 SLC10A2 ATP8MC2 GLRA1 CACNA2D3 SLC6A5
GO:0022890	3.66E-02	9	636	3.129	Inorganic cation transmembrane transporter activity	ATP2C2 SLC32A1 SLC30A3 SLC5A7 CHRNB4 SLC10A2 ATP8MC2 CACNA2D3 SLC6A5
GO:0015370	4.38E-02	3	74	10.517	Solute:sodium symporter activity	SLC5A7 SLC10A2 SLC6A5

ID	Enrichment FDR	nGenes	Pathway Genes	Fold Enrichment	Pathway	Genes
GO:0005102	1.78E-04	37	1722	2.457	Signaling receptor binding	FYN CCDC88C KITLG TRAF3IP2 CASP8 ACTN1 GLG1 BAMBI CCDC88A AAK1 ANGPTL1 CD58 TGFB3 LRP1 NDP APOL2 GFAP WNT2B ANXA1 TMBIM1 TLN1 RIPK1 EGFR RSPO2 BICD1 DBI WIF1 TNFRSF11B ABCA1 STAT3 SMAD2 AKAP5 CSF1 SIPA1L1 CTNND1 DMD EMP2
GO:0005126	1.41E-02	10	327	4.795	Cytokine receptor binding	KITLG CASP8 BAMBI CCDC88A TGFB3 TMBIM1 RIPK1 STAT3 SMAD2 CSF1
GO:0003779	1.98E-02	16	477	2.915	Actin binding	NCK2 WDR1 ACTN1 CAP2 PHACTR2 CCDC88A PALLD FLNB TLN1 EGFR ADD3 WASF2 ANTXR1 SYNPO MRTFA DMD
GO:0008035	1.98E-02	3	11	29.594	High-density lipoprotein particle binding	SCARB1 APOL2 ABCA1
GO:0005109	4.03E-02	4	41	9.865	Frizzled binding	CCDC88C BAMBI NDP WNT2B
GO:0005200	4.03E-02	6	113	5.754	Structural constituent of cytoskeleton	GFAP TLN1 ANK2 ADD3 BICD1 DMD
GO:0017166	4.03E-02	3	12	17.263	Vinculin binding	ACTN1 TLN1 DMD
GO:0030226	4.03E-02	2	3	46.035	Apolipoprotein receptor activity	LRP1 ABCA1
GO:0034185	4.03E-02	3	21	17.263	Apolipoprotein binding	SCARB1 LRP1 ABCA1
GO:0044877	4.03E-02	30	1446	1.934	Protein-containing complex binding	FYN CASP8 NCK2 WDR1 ACTN1 SCARB1 CARMIL1 NOD1 CRYAB SPARC CCDC88A AAK1 TGFB3 LRP1 APOL2 GFAP LCA5 TLN1 RIPK1 ANK2 EGFR ADD3 BICD1 BAG3 SPARCL1 WASF2 ABCA1 ANTXR1 DMD EMP2

Supplementary Figure 4. Intergenic and intronic differential H3K27ac peaks profiling and GO pathway analysis (GO-molecular function). A) Heatmap and **B**) average read density (RPM) profile aggregate plots of H3K27ac signals centered at differential intergenic peaks (center of enhancer ±2 kb flanking region), for heterozygous *AKAP11*-KO clones and WT replicates individually. **C**) Heatmap and **D**) average read density (RPM) profile plots of H3K27ac signals centered at differential intronic peaks (center of enhancer ±2 kb flanking region), for heterozygous *AKAP11*-KO clones and WT replicates individually. **E**) Results table of ORA of reduced intergenic H3K27ac peak intensities associated with decreased gene expression of target genes in heterozygous *AKAP11*-KO vs. WT (intergenic H3K27ac down, expression down: group A), using GO-Molecular Function database. Generated using ShinyGO 0.77; FDR < 0.09; top 20 pathways demonstrated. The background genes used here were the same background gene list (23,590 genes) obtained from our RNA-seq analysis. **F**) GO-Molecular Function ORA of increased intronic H3K27ac peak intensities associated with increased gene expression of target genes in heterozygous *AKAP11*-KO vs. WT (intronic H3K27ac up, expression up group B). Generated using ShinyGO 0.77; FDR < 0.05; top 20 pathways demonstrated. The

background genes used here were the same background gene list (23,590 genes) obtained from our RNA-seq analysis.

Supplementary Tables

Supplementary Table 1. Table of DEG results from RNA-seq data.

Supplementary Table 2. GSEA GO (molecular function) results from heterozygous *AKAP11*-KO vs. WT comparison. Padj<0.05.

Supplementary Table 3. Table of DMRs detected from WGBS data. DMRs were called using the function callDMR at default parameters with a minimum length of 50 base pairs and 3 CpG sites. Annotation determined using Homer (hg38).

Supplementary Table 4. DMR and DEG (p-adj < 0.05 and |log2FC| > 0.25) correlation plot gene list for heterozygous *AKAP11*-KO vs. WT.

Supplementary Table 5. Table of all genes from the correlation plots of differential H3K27ac peaks (p < 0.05 & |Log2FC| > 1) and differential gene expression (adj-p < 0.05 & |Log2FC| > 0.25) in intergenic as well as intronic regions.

Supplementary Table 6. Homer known motif enrichment results. Group A: Total Target Sequences = 188, Total Background Sequences = 49061. Group B: Total Target Sequences = 527, Total Background Sequences = 49150. p=1e-5.

Supplementary Table 7. Table of Differential H3K27ac (adj-P < 0.05 & |log2FC| > 1) and DMR Correlation in intergenic and intronic regions.

ACKNOWLEDGMENTS

The work in G.R.'s lab is supported by the Canadian Institutes of Health Research and ERA PerMed. B.C.'s lab is supported by ERAPerMed PLOT-BD and a grant from the Fondation Bettencourt Schueller. We also acknowledge the financial support from the Brain & Behavior Research Foundation Young Investigator award to A.K. N.F. is supported by the studentship award Fonds de Recherche du Québec – Santé (FRQS). C.L. is supported by the CIHR Banting Fellowship. Computational analysis, data pre-processing, and adapted bioinformatics pipelines for analyses were performed by the Canadian Centre for Computational Genomics (C3G)-Montréal Node (Alain Pacis) using infrastructure provided by Compute Canada and Calcul Quebec. WGBS and ChIP-seq library preparation and sequencing were performed at McGill Genome Center platform. M.A. kindly donated the reprogrammed iPSCs to us.

AUTHOR CONTRIBUTIONS

N.F. and C.L. conceived the study. N.F. designed, defined the scope, and carried out the laboratory experiments. A.K. and Y.L. gave guidance on the iPSC, NPC, and neuronal culture maintenance. N.F. designed and C3G (A.P.) carried out the computational analysis of the data with some guidance from N.F. and A.K. B.C. funded the next-generation sequencings and library preparations and G.R. lab funded the RNA-seq work and both provided guidance. M.A., P.D., G.R., B.C., C.L., and A.K. gave valuable scientific advice during the course of this study. N.F. wrote the manuscript.

DECLARATION OF INTERESTS

The authors declare no competing interests.

RESOURCE AVAILABILITY

LEAD CONTACT

Additional information and requests for resources and reagents should be directed to and will be fulfilled by the Lead Contacts Drs. Rouleau, Khayachi, and Chaumette.

MATERIALS AVAILABILITY

This study did not generate new unique reagents.

References

1 Jann, M. W. Diagnosis and treatment of bipolar disorders in adults: a review of the evidence on pharmacologic treatments. *Am Health Drug Benefits* **7**, 489-499 (2014).

2 Kerner, B. Toward a Deeper Understanding of the Genetics of Bipolar Disorder. *Front Psychiatry* **6**, 105 (2015). https://doi.org/10.3389/fpsyt.2015.00105

3 Palmer, D. S. *et al.* Exome sequencing in bipolar disorder identifies AKAP11 as a risk gene shared with schizophrenia. *Nat Genet* **54**, 541-547 (2022). https://doi.org/10.1038/s41588-022-01034-x

4 Coryell, W. *et al.* The significance of psychotic features in manic episodes: a report from the NIMH collaborative study. *J Affect Disord* **67**, 79-88 (2001). https://doi.org/10.1016/s0165-0327(99)00024-5

5 Kerner, B. Genetics of bipolar disorder. *Appl Clin Genet* **7**, 33-42 (2014). https://doi.org/10.2147/TACG.S39297

6 Ganna, A. *et al.* Quantifying the Impact of Rare and Ultra-rare Coding Variation across the Phenotypic Spectrum. *Am J Hum Genet* **102**, 1204-1211 (2018). https://doi.org/10.1016/j.ajhg.2018.05.002

7 Mullins, N. *et al.* Genome-wide association study of more than 40,000 bipolar disorder cases provides new insights into the underlying biology. *Nat Genet* **53**, 817-829 (2021). https://doi.org/10.1038/s41588-021-00857-4

8 Smith, F. D., Langeberg, L. K. & Scott, J. D. The where's and when's of kinase anchoring. *Trends Biochem Sci* **31**, 316-323 (2006). https://doi.org/10.1016/j.tibs.2006.04.009

9 Bucko, P. J. & Scott, J. D. Drugs That Regulate Local Cell Signaling: AKAP Targeting as a Therapeutic Option. *Annu Rev Pharmacol Toxicol* **61**, 361-379 (2021). https://doi.org/10.1146/annurev-pharmtox-022420-112134

10 Esseltine, J. L. & Scott, J. D. AKAP signaling complexes: pointing towards the next generation of therapeutic targets? *Trends Pharmacol Sci* **34**, 648-655 (2013). https://doi.org/10.1016/j.tips.2013.10.005

11 Wild, A. R. & Dell'Acqua, M. L. Potential for therapeutic targeting of AKAP signaling complexes in nervous system disorders. *Pharmacol Ther* **185**, 99-121 (2018). https://doi.org/10.1016/j.pharmthera.2017.12.004

12 Woolfrey, K. M. & Dell'Acqua, M. L. Coordination of Protein Phosphorylation and Dephosphorylation in Synaptic Plasticity. *J Biol Chem* **290**, 28604-28612 (2015). https://doi.org/10.1074/jbc.R115.657262

13 Shepard, R. D. *et al.* Targeting histone deacetylation for recovery of maternal deprivation-induced changes in BDNF and AKAP150 expression in the VTA. *Exp Neurol* **309**, 160-168 (2018). https://doi.org/10.1016/j.expneurol.2018.08.002

14 Consortium, G. T. The GTEx Consortium atlas of genetic regulatory effects across human tissues. *Science* **369**, 1318-1330 (2020). https://doi.org/10.1126/science.aaz1776

15 Schillace, R. V. & Scott, J. D. Association of the type 1 protein phosphatase PP1 with the A-kinase anchoring protein AKAP220. *Curr Biol* **9**, 321-324 (1999). https://doi.org/10.1016/s0960-9822(99)80141-9

16 Nygren, P. J. & Scott, J. D. Therapeutic strategies for anchored kinases and phosphatases: exploiting short linear motifs and intrinsic disorder. *Front Pharmacol* **6**, 158 (2015). https://doi.org/10.3389/fphar.2015.00158

17 Tanji, C. *et al.* A-kinase anchoring protein AKAP220 binds to glycogen synthase kinase-3beta (GSK-3beta) and mediates protein kinase A-dependent inhibition of GSK-3beta. *J Biol Chem* **277**, 36955-36961 (2002). https://doi.org/10.1074/jbc.M206210200

18 Freland, L. & Beaulieu, J. M. Inhibition of GSK3 by lithium, from single molecules to signaling networks. *Front Mol Neurosci* **5**, 14 (2012). https://doi.org/10.3389/fnmol.2012.00014

19 Kishore, B. K. & Ecelbarger, C. M. Lithium: a versatile tool for understanding renal physiology. *Am J Physiol Renal Physiol* **304**, F1139-1149 (2013). https://doi.org/10.1152/ajprenal.00718.2012

20 Alda, M. Lithium in the treatment of bipolar disorder: pharmacology and pharmacogenetics. *Mol Psychiatry* **20**, 661-670 (2015). https://doi.org/10.1038/mp.2015.4

21 Jope, R. S. Lithium and GSK-3: one inhibitor, two inhibitory actions, multiple outcomes. *Trends Pharmacol Sci* **24**, 441-443 (2003). https://doi.org/10.1016/S0165-6147(03)00206-2

22 Logue, J. S., Whiting, J. L., Tunquist, B., Langeberg, L. K. & Scott, J. D. Anchored protein kinase A recruitment of active Rac GTPase. *J Biol Chem* **286**, 22113-22121 (2011). https://doi.org/10.1074/jbc.M111.232660

23 Schillace, R. V., Voltz, J. W., Sim, A. T., Shenolikar, S. & Scott, J. D. Multiple interactions within the AKAP220 signaling complex contribute to protein phosphatase 1 regulation. *J Biol Chem* **276**, 12128-12134 (2001). https://doi.org/10.1074/jbc.M010398200

24 Steven, A. *et al.* What turns CREB on? And off? And why does it matter? *Cell Mol Life Sci* **77**, 4049-4067 (2020). https://doi.org/10.1007/s00018-020-03525-8

25 Ha, C. H. *et al.* PKA phosphorylates histone deacetylase 5 and prevents its nuclear export, leading to the inhibition of gene transcription and cardiomyocyte hypertrophy. *Proc Natl Acad Sci U S A* **107**, 15467-15472 (2010). https://doi.org/10.1073/pnas.1000462107

26 Chen, S., Owens, G. C., Makarenkova, H. & Edelman, D. B. HDAC6 regulates mitochondrial transport in hippocampal neurons. *PLoS One* **5**, e10848 (2010). https://doi.org/10.1371/journal.pone.0010848

27 Abu-Farha, M. *et al.* The tale of two domains: proteomics and genomics analysis of SMYD2, a new histone methyltransferase. *Mol Cell Proteomics* **7**, 560-572 (2008). https://doi.org/10.1074/mcp.M700271-MCP200

28 Ewing, R. M. *et al.* Large-scale mapping of human protein-protein interactions by mass spectrometry. *Mol Syst Biol* **3**, 89 (2007). https://doi.org/10.1038/msb4100134

29 Park, C. Y. *et al.* Tissue-aware data integration approach for the inference of pathway interactions in metazoan organisms. *Bioinformatics* **31**, 1093-1101 (2015). https://doi.org/10.1093/bioinformatics/btu786

30 Szklarczyk, D. *et al.* STRING v10: protein-protein interaction networks, integrated over the tree of life. *Nucleic Acids Res* **43**, D447-452 (2015). https://doi.org/10.1093/nar/gku1003

31 Herzog, L. E. *et al.* Mouse mutants in schizophrenia risk genes GRIN2A and AKAP11 show EEG abnormalities in common with schizophrenia patients. *Transl Psychiatry* **13**, 92 (2023). https://doi.org/10.1038/s41398-023-02393-7

32 Tekell, J. L. *et al.* High frequency EEG activity during sleep: characteristics in schizophrenia and depression. *Clin EEG Neurosci* **36**, 25-35 (2005). https://doi.org/10.1177/155005940503600107

33 Tanaka-Koshiyama, K. *et al.* Abnormal Spontaneous Gamma Power Is Associated With Verbal Learning and Memory Dysfunction in Schizophrenia. *Front Psychiatry* **11**, 832 (2020). https://doi.org/10.3389/fpsyt.2020.00832

34 Aryal, S. *et al.* Deep proteomics identifies shared molecular pathway alterations in synapses of patients with schizophrenia and bipolar disorder and mouse model. *Cell Rep* **42**, 112497 (2023). https://doi.org/10.1016/j.celrep.2023.112497

35 Stern, S. *et al.* Mechanisms Underlying the Hyperexcitability of CA3 and Dentate Gyrus Hippocampal Neurons Derived From Patients With Bipolar Disorder. *Biol Psychiatry* **88**, 139-149 (2020). https://doi.org/10.1016/j.biopsych.2019.09.018

36 Stern, S. *et al.* Neurons derived from patients with bipolar disorder divide into intrinsically different sub-populations of neurons, predicting the patients' responsiveness to lithium. *Mol Psychiatry* **23**, 1453-1465 (2018). https://doi.org/10.1038/mp.2016.260

37 Bolger, A. M., Lohse, M. & Usadel, B. Trimmomatic: a flexible trimmer for Illumina sequence data. *Bioinformatics* **30**, 2114-2120 (2014). https://doi.org/10.1093/bioinformatics/btu170

38 Dobin, A. *et al.* STAR: ultrafast universal RNA-seq aligner. *Bioinformatics* **29**, 15-21 (2013). https://doi.org/10.1093/bioinformatics/bts635

39 Anders, S., Pyl, P. T. & Huber, W. HTSeq--a Python framework to work with high-throughput sequencing data. *Bioinformatics* **31**, 166-169 (2015). https://doi.org/10.1093/bioinformatics/btu638

40 Robinson, M. D., McCarthy, D. J. & Smyth, G. K. edgeR: a Bioconductor package for differential expression analysis of digital gene expression data. *Bioinformatics* **26**, 139-140 (2010). https://doi.org/10.1093/bioinformatics/btp616

41 Ritchie, M. E. *et al.* limma powers differential expression analyses for RNA-sequencing and microarray studies. *Nucleic Acids Res* **43**, e47 (2015). https://doi.org/10.1093/nar/gkv007

42 Gu, Z. Complex heatmap visualization. *iMeta* **1**, e43 (2022). https://doi.org/https://doi.org/10.1002/imt2.43

43 Ge, S. X., Jung, D. & Yao, R. ShinyGO: a graphical gene-set enrichment tool for animals and plants. *Bioinformatics* **36**, 2628-2629 (2020). https://doi.org/10.1093/bioinformatics/btz931

44 Leek, J. T., Johnson, W. E., Parker, H. S., Jaffe, A. E. & Storey, J. D. The sva package for removing batch effects and other unwanted variation in high-throughput experiments. *Bioinformatics* **28**, 882-883 (2012). https://doi.org/10.1093/bioinformatics/bts034

45 Krueger, F. & Andrews, S. R. Bismark: a flexible aligner and methylation caller for Bisulfite-Seq applications. *Bioinformatics* **27**, 1571-1572 (2011). https://doi.org/10.1093/bioinformatics/btr167

46 Feng, H. & Wu, H. Differential methylation analysis for bisulfite sequencing using DSS. *Quant Biol* **7**, 327-334 (2019). https://doi.org/10.1007/s40484-019-0183-8

47 Heinz, S. *et al.* Simple combinations of lineage-determining transcription factors prime cis-regulatory elements required for macrophage and B cell identities. *Mol Cell* **38**, 576-589 (2010). https://doi.org/10.1016/j.molcel.2010.05.004

48 Li, H. & Durbin, R. Fast and accurate short read alignment with Burrows-Wheeler transform. *Bioinformatics* **25**, 1754-1760 (2009). https://doi.org/10.1093/bioinformatics/btp324

49 Zhang, Y. *et al.* Model-based analysis of ChIP-Seq (MACS). *Genome Biol* **9**, R137 (2008). https://doi.org/10.1186/gb-2008-9-9-r137

50 Ramirez, F., Dundar, F., Diehl, S., Gruning, B. A. & Manke, T. deepTools: a flexible platform for exploring deep-sequencing data. *Nucleic Acids Res* **42**, W187-191 (2014). https://doi.org/10.1093/nar/gku365

51 Hunt, G. J., Freytag, S., Bahlo, M. & Gagnon-Bartsch, J. A. dtangle: accurate and robust cell type deconvolution. *Bioinformatics* **35**, 2093-2099 (2019). https://doi.org/10.1093/bioinformatics/bty926

52 Gillespie, M. *et al.* The reactome pathway knowledgebase 2022. *Nucleic Acids Res* **50**, D687-D692 (2022). https://doi.org/10.1093/nar/gkab1028

53 Fabregat, A. *et al.* Reactome pathway analysis: a high-performance in-memory approach. *BMC Bioinformatics* **18**, 142 (2017). https://doi.org/10.1186/s12859-017-1559-2

54 Moller, T. C. *et al.* Oligomerization of a G protein-coupled receptor in neurons controlled by its structural dynamics. *Sci Rep* **8**, 10414 (2018). https://doi.org/10.1038/s41598-018-28682-6

55 Subramanian, A. *et al.* Gene set enrichment analysis: a knowledge-based approach for interpreting genome-wide expression profiles. *Proc Natl Acad Sci U S A* **102**, 15545-15550 (2005). https://doi.org/10.1073/pnas.0506580102

56 Mootha, V. K. *et al.* PGC-1alpha-responsive genes involved in oxidative phosphorylation are coordinately downregulated in human diabetes. *Nat Genet* **34**, 267-273 (2003). https://doi.org/10.1038/ng1180

57 Ashburner, M. *et al.* Gene ontology: tool for the unification of biology. The Gene Ontology Consortium. *Nat Genet* **25**, 25-29 (2000). https://doi.org/10.1038/75556

58 Gene Ontology, C. The Gene Ontology resource: enriching a GOld mine. *Nucleic Acids Res* **49**, D325-D334 (2021). https://doi.org/10.1093/nar/gkaa1113

59 Zyla, J., Marczyk, M., Weiner, J. & Polanska, J. Ranking metrics in gene set enrichment analysis: do they matter? *BMC Bioinformatics* **18**, 256 (2017). https://doi.org/10.1186/s12859-017-1674-0

60 Farhangdoost, N. *et al.* Chromatin dysregulation associated with NSD1 mutation in head and neck squamous cell carcinoma. *Cell Rep* **34**, 108769 (2021). https://doi.org/10.1016/j.celrep.2021.108769

61 Creyghton, M. P. *et al.* Histone H3K27ac separates active from poised enhancers and predicts developmental state. *Proc Natl Acad Sci U S A* **107**, 21931-21936 (2010). https://doi.org/10.1073/pnas.1016071107

62 Rada-Iglesias, A. *et al.* A unique chromatin signature uncovers early developmental enhancers in humans. *Nature* **470**, 279-283 (2011). https://doi.org/10.1038/nature09692

63 Melgar, M. F., Collins, F. S. & Sethupathy, P. Discovery of active enhancers through bidirectional expression of short transcripts. *Genome Biol* **12**, R113 (2011). https://doi.org/10.1186/gb-2011-12-11-r113

64 Zerbino, D. R., Johnson, N., Juettemann, T., Wilder, S. P. & Flicek, P. WiggleTools: parallel processing of large collections of genome-wide datasets for visualization and statistical analysis. *Bioinformatics* **30**, 1008-1009 (2014). https://doi.org/10.1093/bioinformatics/btt737

65 Zhang, T., Zhang, Z., Dong, Q., Xiong, J. & Zhu, B. Histone H3K27 acetylation is dispensable for enhancer activity in mouse embryonic stem cells. *Genome Biol* **21**, 45 (2020). https://doi.org/10.1186/s13059-020-01957-w

66 Raisner, R. *et al.* Enhancer Activity Requires CBP/P300 Bromodomain-Dependent Histone H3K27 Acetylation. *Cell Rep* **24**, 1722-1729 (2018). https://doi.org/10.1016/j.celrep.2018.07.041

67 Lavarone, E., Barbieri, C. M. & Pasini, D. Dissecting the role of H3K27 acetylation and methylation in PRC2 mediated control of cellular identity. *Nat Commun* **10**, 1679 (2019). https://doi.org/10.1038/s41467-019-09624-w

68 Stadler, M. B. *et al.* DNA-binding factors shape the mouse methylome at distal regulatory regions. *Nature* **480**, 490-495 (2011). https://doi.org/10.1038/nature10716

69 Hartl, D., Krebs, A. R., Juttner, J., Roska, B. & Schubeler, D. Cis-regulatory landscapes of four cell types of the retina. *Nucleic Acids Res* **45**, 11607-11621 (2017). https://doi.org/10.1093/nar/gkx923

70 Ziller, M. J. *et al.* Charting a dynamic DNA methylation landscape of the human genome. *Nature* **500**, 477-481 (2013). https://doi.org/10.1038/nature12433

71 Hodges, E. *et al.* Directional DNA methylation changes and complex intermediate states accompany lineage specificity in the adult hematopoietic compartment. *Mol Cell* **44**, 17-28 (2011). https://doi.org/10.1016/j.molcel.2011.08.026

72 Kreibich, E., Kleinendorst, R., Barzaghi, G., Kaspar, S. & Krebs, A. R. Single-molecule footprinting identifies context-dependent regulation of enhancers by DNA methylation. *Mol Cell* **83**, 787-802 e789 (2023). https://doi.org/10.1016/j.molcel.2023.01.017

73 Marmorstein, R. & Zhou, M. M. Writers and readers of histone acetylation: structure, mechanism, and inhibition. *Cold Spring Harb Perspect Biol* **6**, a018762 (2014). https://doi.org/10.1101/cshperspect.a018762

74 Fahira, A., Zhang, J., Xuemin, J., Li, Z. & Shi, Y. Prediction of functional regulatory elements of bipolar disorder via data integration analysis. *Journal of Affective Disorders Reports* **1**, 100015 (2020). https://doi.org/https://doi.org/10.1016/j.jadr.2020.100015

75 Hou, L. *et al.* Genome-wide association study of 40,000 individuals identifies two novel loci associated with bipolar disorder. *Hum Mol Genet* **25**, 3383-3394 (2016). https://doi.org/10.1093/hmg/ddw181

76 Taylor, S. S. *et al.* Signaling through cAMP and cAMP-dependent protein kinase: diverse strategies for drug design. *Biochim Biophys Acta* **1784**, 16-26 (2008). https://doi.org/10.1016/j.bbapap.2007.10.002

77 Pittenger, C., Nestler, E. J. & Duman, R. S. in *Basic Neurochemistry (Eighth Edition)* (eds Scott T. Brady, George J. Siegel, R. Wayne Albers, & Donald L. Price) 423-441 (Academic Press, 2012).

78 Wang, H., Xu, J., Lazarovici, P., Quirion, R. & Zheng, W. cAMP Response Element-Binding Protein (CREB): A Possible Signaling Molecule Link in the Pathophysiology of Schizophrenia. *Front Mol Neurosci* **11**, 255 (2018). https://doi.org/10.3389/fnmol.2018.00255

79 Deng, Z. *et al.* Selective autophagy of AKAP11 activates cAMP/PKA to fuel mitochondrial metabolism and tumor cell growth. *Proc Natl Acad Sci U S A* **118** (2021). https://doi.org/10.1073/pnas.2020215118

80 Zhang, X. *et al.* Genome-wide analysis of cAMP-response element binding protein occupancy, phosphorylation, and target gene activation in human tissues. *Proc Natl Acad Sci U S A* **102**, 4459-4464 (2005). https://doi.org/10.1073/pnas.0501076102

81 Impey, S. *et al.* Defining the CREB regulon: a genome-wide analysis of transcription factor regulatory regions. *Cell* **119**, 1041-1054 (2004). https://doi.org/10.1016/j.cell.2004.10.032

82 Horbach, T., Gotz, C., Kietzmann, T. & Dimova, E. Y. Protein kinases as switches for the function of upstream stimulatory factors: implications for tissue injury and cancer. *Front Pharmacol* **6**, 3 (2015). https://doi.org/10.3389/fphar.2015.00003

83 McKinsey, T. A., Zhang, C. L., Lu, J. & Olson, E. N. Signal-dependent nuclear export of a histone deacetylase regulates muscle differentiation. *Nature* **408**, 106-111 (2000). https://doi.org/10.1038/35040593

84 Grunstein, M. Histone acetylation in chromatin structure and transcription. *Nature* **389**, 349-352 (1997). https://doi.org/10.1038/38664

85 Gopalan, J. *et al.* Targeting an anchored phosphatase-deacetylase unit restores renal ciliary homeostasis. *Elife* **10** (2021). https://doi.org/10.7554/eLife.67828

86 Dai, P. *et al.* CBP as a transcriptional coactivator of c-Myb. *Genes Dev* **10**, 528-540 (1996). https://doi.org/10.1101/gad.10.5.528

87 Schoof, M. *et al.* The transcriptional coactivator and histone acetyltransferase CBP regulates neural precursor cell development and migration. *Acta Neuropathol Commun* **7**, 199 (2019). https://doi.org/10.1186/s40478-019-0849-5

88 Bartal, G., Yitzhaky, A., Segev, A. & Hertzberg, L. Multiple genes encoding mitochondrial ribosomes are downregulated in brain and blood samples of individuals with schizophrenia. *World J Biol Psychiatry*, 1-9 (2023). https://doi.org/10.1080/15622975.2023.2211653

89 Castellanos, M., Gubern, C. & Kadar, E. in *Molecules to Medicine with mTOR* (ed Kenneth Maiese) 105-122 (Academic Press, 2016).

90 Huang, G., Li, H. & Zhang, H. Abnormal Expression of Mitochondrial Ribosomal Proteins and Their Encoding Genes with Cell Apoptosis and Diseases. *Int J Mol Sci* **21** (2020). https://doi.org/10.3390/ijms21228879

91 Li, Z., Okamoto, K., Hayashi, Y. & Sheng, M. The importance of dendritic mitochondria in the morphogenesis and plasticity of spines and synapses. *Cell* **119**, 873-887 (2004). https://doi.org/10.1016/j.cell.2004.11.003

92 Rangaraju, V., Lauterbach, M. & Schuman, E. M. Spatially Stable Mitochondrial Compartments Fuel Local Translation during Plasticity. *Cell* **176**, 73-84 e15 (2019). https://doi.org/10.1016/j.cell.2018.12.013

93 Zhang, X. *et al.* Ribosomal dysregulation: A conserved pathophysiological mechanism in human depression and mouse chronic stress. *PNAS Nexus* **2**, pgad299 (2023). https://doi.org/10.1093/pnasnexus/pgad299

94 Aryal, S. & Klann, E. Turning up translation in fragile X syndrome. *Science* **361**, 648-649 (2018). https://doi.org/10.1126/science.aau6450

95 Aryal, S., Longo, F. & Klann, E. Genetic removal of p70 S6K1 corrects coding sequence length-dependent alterations in mRNA translation in fragile X syndrome mice. *Proc Natl Acad Sci U S A* **118** (2021). https://doi.org/10.1073/pnas.2001681118

96 Niemsiri, V. *et al.* Focal adhesion is associated with lithium response in bipolar disorder: evidence from a network-based multi-omics analysis. *Mol Psychiatry* (2023). https://doi.org/10.1038/s41380-022-01909-9

97 Ou, A. H. *et al.* Lithium response in bipolar disorder is associated with focal adhesion and PI3K-Akt networks: a multi-omics replication study. *Transl Psychiatry* **14**, 109 (2024). https://doi.org/10.1038/s41398-024-02811-4

98 Noritake, J., Watanabe, T., Sato, K., Wang, S. & Kaibuchi, K. IQGAP1: a key regulator of adhesion and migration. *J Cell Sci* **118**, 2085-2092 (2005). https://doi.org/10.1242/jcs.02379

99 Johnson, M., Sharma, M. & Henderson, B. R. IQGAP1 regulation and roles in cancer. *Cell Signal* **21**, 1471-1478 (2009). https://doi.org/10.1016/j.cellsig.2009.02.023

100 Logue, J. S. *et al.* AKAP220 protein organizes signaling elements that impact cell migration. *J Biol Chem* **286**, 39269-39281 (2011). https://doi.org/10.1074/jbc.M111.277756

101 Pantazopoulos, H. *et al.* Molecular signature of extracellular matrix pathology in schizophrenia. *Eur J Neurosci* **53**, 3960-3987 (2021). https://doi.org/10.1111/ejn.15009

102 Matthews, P. R., Eastwood, S. L. & Harrison, P. J. Reduced myelin basic protein and actin-related gene expression in visual cortex in schizophrenia. *PLoS One* **7**, e38211 (2012). https://doi.org/10.1371/journal.pone.0038211

103 Tee, J. Y., Sutharsan, R., Fan, Y. & Mackay-Sim, A. Cell migration in schizophrenia: Patient-derived cells do not regulate motility in response to extracellular matrix. *Mol Cell Neurosci* **80**, 111-122 (2017). https://doi.org/10.1016/j.mcn.2017.03.005

104 Kahler, A. K. *et al.* Association analysis of schizophrenia on 18 genes involved in neuronal migration: MDGA1 as a new susceptibility gene. *Am J Med Genet B Neuropsychiatr Genet* **147B**, 1089-1100 (2008). https://doi.org/10.1002/ajmg.b.30726

105 Gilman, S. R. *et al.* Diverse types of genetic variation converge on functional gene networks involved in schizophrenia. *Nat Neurosci* **15**, 1723-1728 (2012). https://doi.org/10.1038/nn.3261

106 Fromer, M. *et al.* De novo mutations in schizophrenia implicate synaptic networks. *Nature* **506**, 179-184 (2014). https://doi.org/10.1038/nature12929

107 Zhao, Z. *et al.* Transcriptome sequencing and genome-wide association analyses reveal lysosomal function and actin cytoskeleton remodeling in schizophrenia and bipolar disorder. *Mol Psychiatry* **20**, 563-572 (2015). https://doi.org/10.1038/mp.2014.82

108 Schmitt, A. *et al.* Structural synaptic elements are differentially regulated in superior temporal cortex of schizophrenia patients. *Eur Arch Psychiatry Clin Neurosci* **262**, 565-577 (2012). https://doi.org/10.1007/s00406-012-0306-y

109 Cristino, A. S. *et al.* Neurodevelopmental and neuropsychiatric disorders represent an interconnected molecular system. *Mol Psychiatry* **19**, 294-301 (2014). https://doi.org/10.1038/mp.2013.16

110 Prieto, G. A. & Cotman, C. W. Cytokines and cytokine networks target neurons to modulate long-term potentiation. *Cytokine Growth Factor Rev* **34**, 27-33 (2017). https://doi.org/10.1016/j.cytogfr.2017.03.005

111 Momtazmanesh, S., Zare-Shahabadi, A. & Rezaei, N. Cytokine Alterations in Schizophrenia: An Updated Review. *Front Psychiatry* **10**, 892 (2019). https://doi.org/10.3389/fpsyt.2019.00892

112 Lesh, T. A. *et al.* Cytokine alterations in first-episode schizophrenia and bipolar disorder: relationships to brain structure and symptoms. *J Neuroinflammation* **15**, 165 (2018). https://doi.org/10.1186/s12974-018-1197-2

113 Dowlati, Y. *et al.* A meta-analysis of cytokines in major depression. *Biol Psychiatry* **67**, 446-457 (2010). https://doi.org/10.1016/j.biopsych.2009.09.033

114 Miller, B. J., Buckley, P., Seabolt, W., Mellor, A. & Kirkpatrick, B. Meta-analysis of cytokine alterations in schizophrenia: clinical status and antipsychotic effects. *Biol Psychiatry* **70**, 663-671 (2011). https://doi.org/10.1016/j.biopsych.2011.04.013

115 Modabbernia, A., Taslimi, S., Brietzke, E. & Ashrafi, M. Cytokine alterations in bipolar disorder: a meta-analysis of 30 studies. *Biol Psychiatry* **74**, 15-25 (2013). https://doi.org/10.1016/j.biopsych.2013.01.007

116 Munkholm, K., Vinberg, M. & Vedel Kessing, L. Cytokines in bipolar disorder: a systematic review and meta-analysis. *J Affect Disord* **144**, 16-27 (2013). https://doi.org/10.1016/j.jad.2012.06.010

117 Potvin, S. *et al.* Inflammatory cytokine alterations in schizophrenia: a systematic quantitative review. *Biol Psychiatry* **63**, 801-808 (2008). https://doi.org/10.1016/j.biopsych.2007.09.024

118 Upthegrove, R., Manzanares-Teson, N. & Barnes, N. M. Cytokine function in medication-naive first episode psychosis: a systematic review and meta-analysis. *Schizophr Res* **155**, 101-108 (2014). https://doi.org/10.1016/j.schres.2014.03.005

119 Goldsmith, D. R., Rapaport, M. H. & Miller, B. J. A meta-analysis of blood cytokine network alterations in psychiatric patients: comparisons between schizophrenia, bipolar disorder and depression. *Mol Psychiatry* **21**, 1696-1709 (2016). https://doi.org/10.1038/mp.2016.3

120 Rizzardi, L. F. *et al.* Neuronal brain-region-specific DNA methylation and chromatin accessibility are associated with neuropsychiatric trait heritability. *Nat Neurosci* **22**, 307-316 (2019). https://doi.org/10.1038/s41593-018-0297-8

121 Yao, P. *et al.* Coexpression networks identify brain region-specific enhancer RNAs in the human brain. *Nat Neurosci* **18**, 1168-1174 (2015). https://doi.org/10.1038/nn.4063

122 Hannon, E., Marzi, S. J., Schalkwyk, L. S. & Mill, J. Genetic risk variants for brain disorders are enriched in cortical H3K27ac domains. *Mol Brain* **12**, 7 (2019). https://doi.org/10.1186/s13041-019-0429-4

123 Girdhar, K. *et al.* Chromatin domain alterations linked to 3D genome organization in a large cohort of schizophrenia and bipolar disorder brains. *Nat Neurosci* **25**, 474-483 (2022). https://doi.org/10.1038/s41593-022-01032-6

124 Selleri, L. *et al.* The TALE homeodomain protein Pbx2 is not essential for development and long-term survival. *Mol Cell Biol* **24**, 5324-5331 (2004). https://doi.org/10.1128/MCB.24.12.5324-5331.2004

125 Lin, J. *et al.* Coexpression of HOXA6 and PBX2 promotes metastasis in gastric cancer. *Aging (Albany NY)* **13**, 6606-6624 (2021). https://doi.org/10.18632/aging.202426

126 Autism Spectrum Disorders Working Group of The Psychiatric Genomics, C. Meta-analysis of GWAS of over 16,000 individuals with autism spectrum disorder highlights a novel locus at

10q24.32 and a significant overlap with schizophrenia. *Mol Autism* **8**, 21 (2017). https://doi.org/10.1186/s13229-017-0137-9

127 Saito, T. *et al.* Pharmacogenomic Study of Clozapine-Induced Agranulocytosis/Granulocytopenia in a Japanese Population. *Biol Psychiatry* **80**, 636-642 (2016). https://doi.org/10.1016/j.biopsych.2015.12.006

128 Blomquist, P., Belikov, S. & Wrange, O. Increased nuclear factor 1 binding to its nucleosomal site mediated by sequence-dependent DNA structure. *Nucleic Acids Res* **27**, 517-525 (1999). https://doi.org/10.1093/nar/27.2.517

129 Wang, W. *et al.* A role for nuclear factor I in the intrinsic control of cerebellar granule neuron gene expression. *J Biol Chem* **279**, 53491-53497 (2004). https://doi.org/10.1074/jbc.M410370200

130 Furlong, E. E., Keon, N. K., Thornton, F. D., Rein, T. & Martin, F. Expression of a 74-kDa nuclear factor 1 (NF1) protein is induced in mouse mammary gland involution. Involution-enhanced occupation of a twin NF1 binding element in the testosterone-repressed prostate message-2/clusterin promoter. *J Biol Chem* **271**, 29688-29697 (1996). https://doi.org/10.1074/jbc.271.47.29688

131 Kawamura, H., Nagata, K., Masamune, Y. & Nakanishi, Y. Phosphorylation of NF-I in vitro by cdc2 kinase. *Biochem Biophys Res Commun* **192**, 1424-1431 (1993). https://doi.org/10.1006/bbrc.1993.1575

132 Reifel-Miller, A. E., Calnek, D. S. & Grinnell, B. W. Tyrosine phosphorylation regulates the DNA binding activity of a nuclear factor 1-like repressor protein. *Journal of Biological Chemistry* **269**, 23861-23864 (1994). https://doi.org/https://doi.org/10.1016/S0021-9258(19)51015-8

133 Nebl, G., Mermod, N. & Cato, A. C. Post-transcriptional down-regulation of expression of transcription factor NF1 by Ha-ras oncogene. *Journal of Biological Chemistry* **269**, 7371-7378 (1994). https://doi.org/https://doi.org/10.1016/S0021-9258(17)37294-0

134 Streuli, C. H. *et al.* Stat5 as a target for regulation by extracellular matrix. *J Biol Chem* **270**, 21639-21644 (1995). https://doi.org/10.1074/jbc.270.37.21639

135 Jope, R. S. *et al.* The phosphoinositide signal transduction system is impaired in bipolar affective disorder brain. *J Neurochem* **66**, 2402-2409 (1996). https://doi.org/10.1046/j.1471-4159.1996.66062402.x

136 Gould, T. D. & Manji, H. K. Signaling networks in the pathophysiology and treatment of mood disorders. *J Psychosom Res* **53**, 687-697 (2002). https://doi.org/10.1016/s0022-3999(02)00426-9

137 Catapano, L. A. & Manji, H. K. G protein-coupled receptors in major psychiatric disorders. *Biochim Biophys Acta* **1768**, 976-993 (2007). https://doi.org/10.1016/j.bbamem.2006.09.025

138 Subramaniam, M., Abdin, E., Vaingankar, J. A. & Chong, S. A. Prevalence, correlates, comorbidity and severity of bipolar disorder: results from the Singapore Mental Health Study. *J Affect Disord* **146**, 189-196 (2013). https://doi.org/10.1016/j.jad.2012.09.002

139 Cruceanu, C. *et al.* Rare susceptibility variants for bipolar disorder suggest a role for G protein-coupled receptors. *Mol Psychiatry* **23**, 2050-2056 (2018). https://doi.org/10.1038/mp.2017.223

140 Boczek, T. *et al.* The Role of G Protein-Coupled Receptors (GPCRs) and Calcium Signaling in Schizophrenia. Focus on GPCRs Activated by Neurotransmitters and Chemokines. *Cells* **10** (2021). https://doi.org/10.3390/cells10051228

141 Bosse, A. *et al.* Identification of the vertebrate Iroquois homeobox gene family with overlapping expression during early development of the nervous system. *Mech Dev* **69**, 169-181 (1997). https://doi.org/10.1016/s0925-4773(97)00165-2

142 Ahn, J. I. *et al.* Comprehensive transcriptome analysis of differentiation of embryonic stem cells into midbrain and hindbrain neurons. *Dev Biol* **265**, 491-501 (2004). https://doi.org/10.1016/j.ydbio.2003.09.041

143 Kasper, C., Hebert, F. O., Aubin-Horth, N. & Taborsky, B. Divergent brain gene expression profiles between alternative behavioural helper types in a cooperative breeder. *Mol Ecol* **27**, 4136-4151 (2018). https://doi.org/10.1111/mec.14837

144 Tena, J. J. *et al.* An evolutionarily conserved three-dimensional structure in the vertebrate Irx clusters facilitates enhancer sharing and coregulation. *Nat Commun* **2**, 310 (2011). https://doi.org/10.1038/ncomms1301

145 Gomez-Velazquez, M. *et al.* CTCF counter-regulates cardiomyocyte development and maturation programs in the embryonic heart. *PLoS Genet* **13**, e1006985 (2017). https://doi.org/10.1371/journal.pgen.1006985

146 Vaillancourt, K. *et al.* Cocaine-related DNA methylation in caudate neurons alters 3D chromatin structure of the IRXA gene cluster. *Mol Psychiatry* **26**, 3134-3151 (2021). https://doi.org/10.1038/s41380-020-00909-x

147 Hashimoto, H. *et al.* Structural Basis for the Versatile and Methylation-Dependent Binding of CTCF to DNA. *Mol Cell* **66**, 711-720 e713 (2017). https://doi.org/10.1016/j.molcel.2017.05.004

148 Maurano, M. T. *et al.* Role of DNA Methylation in Modulating Transcription Factor Occupancy. *Cell Rep* **12**, 1184-1195 (2015). https://doi.org/10.1016/j.celrep.2015.07.024

149 Kakinuma, N., Roy, B. C., Zhu, Y., Wang, Y. & Kiyama, R. Kank regulates RhoA-dependent formation of actin stress fibers and cell migration via 14-3-3 in PI3K-Akt signaling. *J Cell Biol* **181**, 537-549 (2008). https://doi.org/10.1083/jcb.200707022

150 Roy, B. C., Kakinuma, N. & Kiyama, R. Kank attenuates actin remodeling by preventing interaction between IRSp53 and Rac1. *J Cell Biol* **184**, 253-267 (2009). https://doi.org/10.1083/jcb.200805147

151 Gee, H. Y. *et al.* KANK deficiency leads to podocyte dysfunction and nephrotic syndrome. *J Clin Invest* **125**, 2375-2384 (2015). https://doi.org/10.1172/JCI79504

152 Jensen, M. & Girirajan, S. Mapping a shared genetic basis for neurodevelopmental disorders. *Genome Med* **9**, 109 (2017). https://doi.org/10.1186/s13073-017-0503-4

153 Romanos, M. *et al.* Genome-wide linkage analysis of ADHD using high-density SNP arrays: novel loci at 5q13.1 and 14q12. *Mol Psychiatry* **13**, 522-530 (2008). https://doi.org/10.1038/mp.2008.12

154 Larsson, H. *et al.* Risk of bipolar disorder and schizophrenia in relatives of people with attention-deficit hyperactivity disorder. *Br J Psychiatry* **203**, 103-106 (2013). https://doi.org/10.1192/bjp.bp.112.120808

155 Sutton, G. J. *et al.* Comprehensive evaluation of deconvolution methods for human brain gene expression. *Nat Commun* **13**, 1358 (2022). https://doi.org/10.1038/s41467-022-28655-4